2D Materials for 1D Electrochemical Energy Storage Devices

Shengli Zhai[a,b], Li Wei[a], H. Enis Karahan[b], Xuncai Chen[a], Chaojun Wang[a], Xinshi Zhang[a], Junsheng Chen[a], Xin Wang[b] and Yuan Chen[a,□]

[a] The University of Sydney, School of Chemical and Biomolecular Engineering, Sydney, New South Wales 2006, Australia

[b] Nanyang Technological University, School of Chemical and Biomedical Engineering, 62 Nanyang Drive, 637459, Singapore

□ Corresponding authors.

E-mail address: yuan.chen@sydney.edu.au (Y. Chen)

2D Materials for 1D Electrochemical Energy Storage Devices

Contents

Abstract

1D electrochemical energy storage devices, such as fiber supercapacitors and cable-shaped batteries, are promising energy storage solutions for emerging wearable electronics due to their advantages in flexibility, weavability, and wearability. 2D materials with unique structures and properties can be used to create novel 1D electrochemical energy storage devices. Here, we reviewed recent research efforts in using various 2D materials, such as graphene, transitional metal dichalcogenides, transition metal oxides, transition metal hydroxides, and transitional metal carbides and carbonitrides, to construct fiber supercapacitors and cable-shaped batteries. For every 2D material, we first examined its intrinsic properties and their impacts on its energy storage performance. Next, we reviewed several universal approaches which have been used to enhance its performance, including creating nanostructures, controlling the stacking/alignment, modulating chemical properties via doping or phase engineering, forming nanocomposites to increase electrical conductivity or stability, and designing fiber/cable electrode architectures. Further, we also compared the key characteristics and energy storage performance of recently reported 1D electrochemical energy storage devices containing 2D materials. Last, we offer our perspectives on the challenges and potential future research directions in this area. We hope this review can stimulate more research to realize the applications of 2D materials in practical 1D electrochemical energy storage devices.

Keywords: 2D material, 1D electrochemical energy storage device, fiber supercapacitor, cable-shaped battery

1. Introduction

Wearable devices are a new class of clothing and accessories incorporated with electronic components or mini-computers that can be comfortably worn on the body.[1, 2] Smart tattoos or body implants are more invasive forms of wearable devices.[3, 4] They enable seamless access to electronics/computer interfaces and provide smart functions, such as tracking physiological conditions of the body, or sensing and responding to various environmental stimuli from different sources.[5, 6] They can also be connected to the Internet through wireless or mobile networks, enabling data exchanges with other users. The growing consumer interests, the fast improvement in electronic technologies, and the booming of the Internet mobility industry synergistically facilitate the recent fast development in wearable devices, such as Apple watches, Huawei wristbands, and Sony VR headsets. They are playing important roles in fitness and sports monitoring, education, entertainment, fashion, medical and healthcare, as well as potential military applications. More and more components are being integrated to achieve multiple functions, which creates a strong demand for stable and long-lasting energy storage solution. Further, a new generation of wearable devices also demands enhanced wearability. For example, they might be directly worn on a large area of soft, curved, and stretchable skin similar to traditional textiles.[7-10] However, current wearable devices are typically powered by rigid electrochemical energy storage devices, including lithium-ion batteries (LIBs) and supercapacitors (SCs). All components of these electrochemical energy storage devices are sealed inside metallic or plastic casings to ensure their safe operation. They are often large and heavy without mechanical flexibility. Thus, they are not comparable to the new generation of wearable devices.[10-12]

An emerging energy storage solution for wearable devices is using 1D electrochemical energy storage devices, including fiber supercapacitors (FSCs) and cable-shaped batteries (CBs). Compared to conventional SCs and batteries, 1D electrochemical energy storage

devices have several potential advantages originated from their 1D cylindrically shaped structures: (1) they are mechanically flexible and deformable under various bending and twisting conditions, enabling better wearability.[13] (2) Long and multiple 1D fibers/cables may be integrated into flexible textiles using knitting/weaving textile techniques to create large area textile-based electrochemical energy storage devices.[10] (3) 1D fibers/cables may be assembled into various shapes, and placed at different desirable locations in wearable devices, which enable a greater design versatility.[10, 11] (4) They may be further integrated with 1D energy harvesting devices or other 1D devices, such as displays and sensors, to create multifunctional wearable systems.[10, 13, 14]

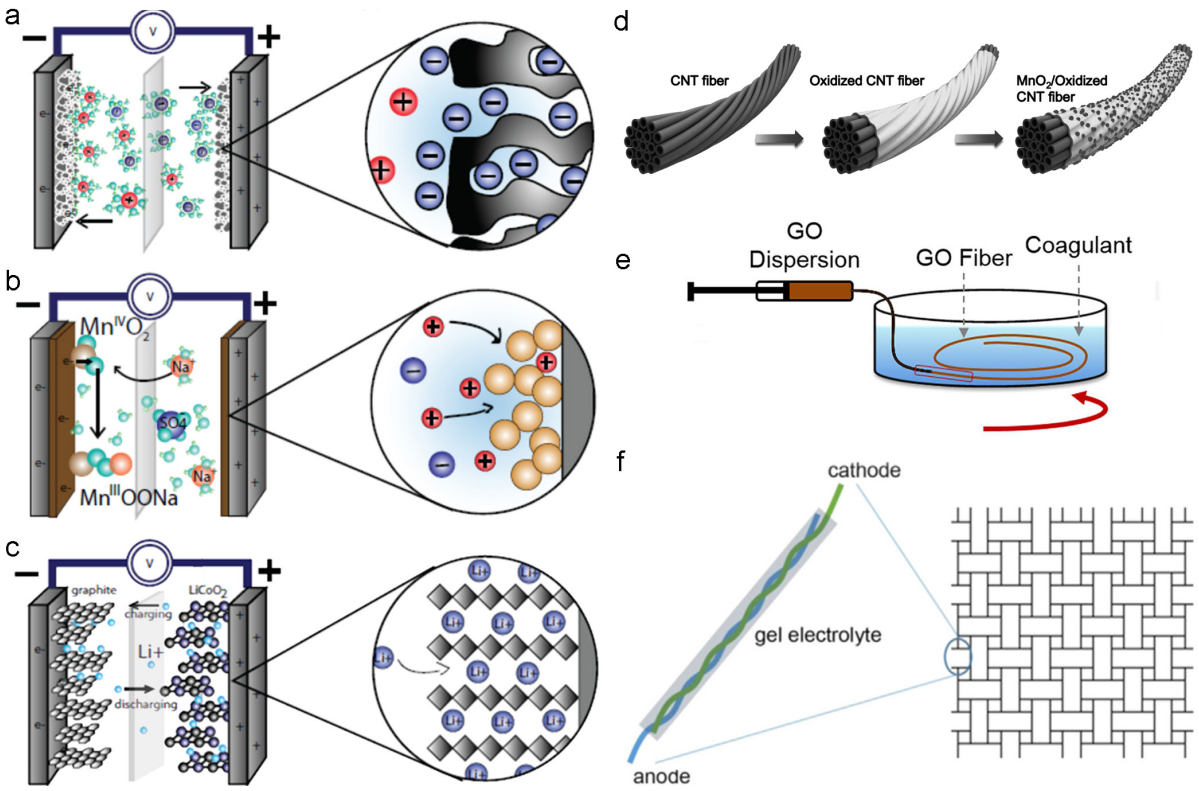

Fig. 1. Schematic illustration of the energy storage mechanisms in common electrochemical energy storage devices: (a) a supercapacitor based on electrical double layer capacitance, (b) a supercapacitor based on pseudocapacitance and (c) a Li-ion battery. Reproduced with permission.[13] Copyright 2014, Royal Society of Chemistry (RSC). (d) Schematic

illustration of directly depositing nanostructured MnO_2 on existing CNT fibers via a solution process, (e) the wet-spinning of GO dispersion into freestanding GO fiber to create fiber/cable electrodes for fabricating 1D electrochemical energy storage devices. Reproduced with permission.[15, 16] Copyright 2017, Wiley-VCH. Copyright 2015, Springer Nature. (f) Schematic illustration of an individual 1D electrochemical energy storage device (left) and an energy storage textile integrated by weaving multiple 1D electrochemical energy storage devices. Reproduced with permission.[11] Copyright 2016, Elsevier.

SCs typically comprise a positive electrode, a negative electrode, a separator and an electrolyte (Fig. 1a, b). They store electrical energy through electrochemical double layer capacitance (EDLC) by reversible electrolyte ion adsorption at the surface or inside pores of electrodes and pseudocapacitance through surface redox reactions or intercalation at electrode surfaces. In general, high-performance SCs require electrode materials which have (1) a large specific surface area and excellent surface wettability for adsorption of electrolyte ions, (2) abundant pores with a hierarchical pore size distribution and interconnected pore connections for efficient electrolyte ion diffusion, (3) a high electrical conductivity for fast electron transfer, and (4) high pseudocapacitance to enable higher specific energy storage density.[17, 18] Batteries usually consist of an anode and a cathode separated by an electrolyte-filled separator. They store energy via different faradic reactions taking place on the electrodes, which are usually accompanied by a phase transformation in the electrode materials. For example, LIBs (Fig. 1c) store energy by the insertion of Li^+ ions from the anode to the cathode when discharging or moving backward when charging. Some common requirements for battery electrode materials include: (1) an excellent reversible energy storage capacity and a suitable operating voltage window to enable high energy storage density, (2) a high electron and ion transport mobility to deliver a high power, and (3) an excellent structural stability

upon phase transformations during faradic reactions over many charging/discharging cycles to enable a long battery life.[19, 20]

Electrode materials can be directly deposited on existing 1D conductive fibers/cables to create fiber/cable electrodes for fabricating 1D FSCs or CBs (see a representative sample of depositing MnO_2 on carbon nanotube (CNT) fibers illustrated in Fig. 1d). Alternatively, electrode materials and other materials can be directly assembled from a bottom-up approach to form freestanding fiber/cable electrodes (see a representative sample of assembling graphene oxide (GO) nanosheets into GO fibers in Fig. 1e). The length of fiber/cable electrodes may range from several millimeters to meters. Electrons are often required to travel a long distance along the axial direction to reach external circuits. In contrast, electrons only need to pass through the thickness of electrode materials on current collectors in conventional planar devices, which are usually several orders smaller, ranging from several nanometers to hundreds of micrometers. Because the required electron transfer distance in FSCs or CBs is significantly longer, fiber/cable electrodes need to have an excellent electrical conductivity to deliver a good energy storage performance. Besides, the wearability recruitments of FSCs or CBs also demand excellent mechanical flexibility and good safety for electrode materials.

Because most of the commonly used electrode materials cannot satisfy the requirements above by FSCs and CBs, substantial research efforts have recently been devoted to exploring new materials. Since the discovery of 2D graphene in 2004,[21] significant progress has been made in the synthesis and applications of graphene-family materials in various fields.[22-24] The success of graphene also inspired the exploration of other 2D materials, which are atomically thin, layered crystalline solids with covalent bonds within each layer and van der Waals forces among interlayers.[25] Currently studied 2D materials include graphene, some

2D transitional metal dichalcogenides (TMDs), transition metal oxides (TMOs), transition metal hydroxides (TMHs), and transitional metal carbides and carbonitrides (MXenes).[26-29]

In comparison to bulky materials, 2D materials offer some unique advantages as electrode materials. (1) Their high surface-to-volume ratio provides a large specific surface area. (2) The abundant active sites can be created on their edges and basal planes, which may increase their energy storage capacity. (3) Their layered structure may shorten the diffusion pathway of electrolyte ions, resulting in higher ionic conductivity. (4) The space between their layers may enable ion intercalation for some energy storage devices, such as LIBs, sodium-ion batteries (NIBs), and intercalation-type SCs.[28-32] (5) 2D materials can also provide additional beneficial characteristics for fiber-based energy storage devices, for example, some of them are mechanically strong and flexible, suitable for fabricating flexible devices. (6) Some 2D materials, such as graphene, metallic MXenes, and 1T TMDs, have high electrical conductivity, which enables a fast electron transfer in 1D electrodes.[26, 28-34] Although some 1D materials, such as nanotubes and nanowires, can also provide a large specific surface area, good mechanical properties, and high electrical conductivity, 2D materials are often superior in many of these aspects mentioned above.

In this review, we first briefly summarize the general development trend of two important components in 1D FSCs and CBs, *i.e.*, fiber/cable substrates and electrolytes. Next, we provide a detailed account of recent advances in applying various 2D materials in FSCs and CBs. Due to their different energy storage mechanisms, our discussions are split into two broad groups, focusing on 1D FSCs and CBs, respectively. Although the research related to different types of 2D materials are reviewed separately, for every material, we usually start with a discussion of its intrinsic properties, such as specific surface area, crystal structures, crystalline phases, interlayer spacings, specific capacitance, and electrical conductivity, and how these properties affect their energy storage performance. Afterward, we discuss several

universal approaches which have been used to enhance the performance of various 2D materials in 1D electrochemical energy storage devices. As shown in Fig. 2, these approaches include (1) engineering 2D materials' physical structures (*e.g.*, specific surface area, particle size, and porosity) by creating nanostructures or controlling their stacking/alignment, (2) modulating their chemical properties, such as heteroatom doping and phase engineering, (3) forming of nanocomposites to increase their electrical conductivity or stability, (4) designing fiber/cable electrodes with various architectures, and (5) achieving scalable and cost-effective manufacture. In several summary tables, we also compare the key characteristics and energy storage performance of recently reported 1D electrochemical energy storage devices containing 2D materials. Last, we offer our perspectives on the challenges and potential future research directions for realizing the applications of 2D materials in practical 1D electrochemical energy storage devices.

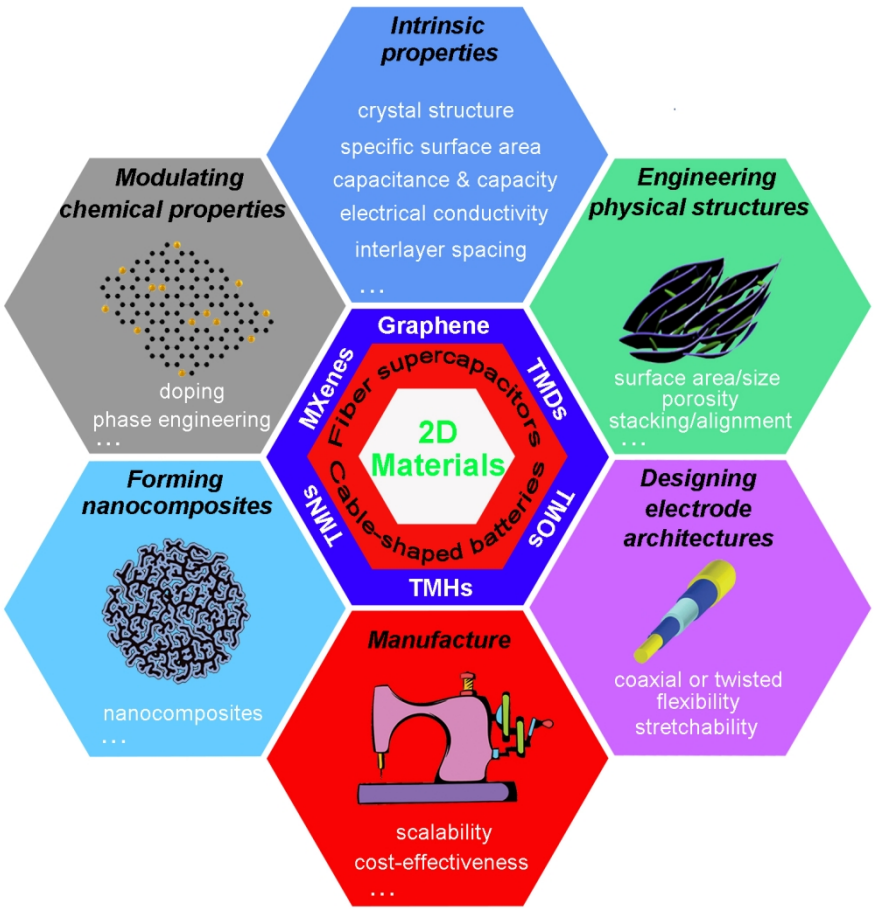

Fig. 2. Some general strategies to enhance the performance of 2D materials in 1D electrochemical energy storage devices.

2. Fiber/cable substrates for 1D fiber supercapacitors and cable-shaped batteries

As described above, the general requirements of fiber/cable substrates for 1D FSCs and CBs includes excellent electrical conductivity to deliver good energy storage performance and mechanical properties to meet different wearing requirements. To date, fiber/cable substrates used to fabricate 1D FSCs and CBs are mainly modified textile yarns, metals wires, and various carbon-based fibers.

Modified textile yarns include natural yarns (*e.g.,* cotton yarns) and synthetic polymetric yarns (*e.g.,* polyester and nylon yarns). The advantages of textiles yarns are their moderate mechanical strength, lightweight, low cost, abundant availability on the market. A commonly used strategy to increase their electrical conductivity is to coat their outer surface with various conductive materials, such as carbon materials, metals or conductive polymers. For example, Liu *et al*. reported a yarn supercapacitor based on commercial cotton threads. SWCNTs were tightly anchored on the surface of the cotton threads via a simple dipping and drying process, yielding an electrical conductivity of 0.05 S cm^{-1}.[35] Zheng *et al.* used nickel coated cotton yarns with a much higher electrical conductivity of 0.625 S cm^{-1}.[36] Other than natural yarns, Kim *et al.* reported a nylon fiber based solid-state FSCs. CNT sheets drawn from MWCNT forests were wrapped on nylon yarns, leading to an electrical conductivity of 0.0052 S cm^{-1}.[37]

There are several obstacles to use modified textile yarns for practical applications. (1) Their electrical conductivity is still insufficient, leading to satisfactory energy storage performance, especially with the extension of the device length. (2) It is not a trivial task to coat conductive materials uniformly on textile yarns. (3) To make conductive materials stable anchored on fiber/yarn substrate, Forming strong interactions between conductive materials and substrates (*e.g.,* van der Waals forces or covalent bonds) is often needed to stably anchor conductive materials on fiber/yarn substrates, which limits the choices of conductive materials.[38]

Because the bending strain of materials is proportional to their thickness, many materials become bendable when their size becomes very thin.[39] Different types of thin metal wires (*e.g.,* stainless steel, Ni, Pt, and Cu wires) with diameters down to micrometers have been used as substrates (current collectors) in 1D FSCs and CBs. In general, metal wires are mechanically robust, and their electrical conductivity is several orders of magnitude higher

than most of modified textiles yarns. The high electrical conductivity is beneficial for delivering excellent rate capability even for devices with a considerable length. The main drawbacks of metal wires include that they are heavy, and some of them can be easily corroded in acidic or basic electrolytes, which restrict their lifetime.

Considerable efforts have also been devoted to exploring various carbon material-based fibers, such as graphitic carbon fibers, CNT fibers, and graphene fibers or CNT/graphene composite fibers. They exhibit similar density and sometimes better mechanical strength compared to textile yarns. Their electrical conductivity is often several orders of magnitude higher than textile yarns. These properties make them excellent candidates as fiber electrodes for 1D electrochemical energy storage devices. Besides, various other electrode materials can be directly integrated into CNT, graphene, and composite fibers using bottom-up synthesis approaches, which provide excellent design versatility. Graphitic carbon fibers are already commercially available in large scale, while CNT fibers and graphene fibers are available in a smaller scale. It is desirable to achieve large scalable production and reduce their costs so they can be used in practical applications.

3. Electrolytes for 1D fiber supercapacitors and cable-shaped batteries

Various liquid or gel electrolytes have been explored to fabricate 1D electrochemical energy storage devices. The desirable characteristics of electrolytes include high ionic conductivity, low/non-toxicity, excellent stability, suitable mechanical flexibility/strength, and low cost. Liquid electrolytes include aqueous, organic electrolytes, and ionic liquids. Gel electrolytes typically comprise of a polymer framework as a host, an organic/aqueous solution as a plasticizer, and salts as an ion donor. In comparison to liquid electrolytes, gel electrolytes are more often used in 1D electrochemical energy storage devices due to their reasons. (1) Gel electrolytes have suitable mechanical properties, which can be easily handled

to create flexible devices without leakage.[40] (2) They can also act as a separator between two electrodes, which simplifies the device fabrication without introducing a separate separator. (3) Many gel electrolytes are non-flammable, have low toxicity, and can work in a wide range of operating temperatures.[41]

The most commonly used polymer frameworks for gel electrolytes include poly(vinyl alcohol) (PVA), polyacrylate (PAA), poly(ethylene oxide) (PEO), polyacrylonitrile (PAN), poly(vinylidene fluoride) (PVDF), poly(methyl methacrylate) (PMMA) and potassium polyacrylate (PAAK). H3PO4, H2SO4, Na2SO4, KOH, and LiCl are often used as ion donors. Currently, PVA-based gel electrolytes are the most widely used gel electrolyte in 1D electrochemical energy storage devices because of the ease of preparation, hydrophilicity, good film-forming properties, non-toxic characteristics, and low cost.[42] However, PVA-based gel electrolytes often suffer from fluidity problems at high temperatures. Some of them (e.g., PVA/KOH) have a short life due to continuous dehydration. Several strategies to addressing these issues and new types of gel electrolytes are discussed in a recent review article.[42]

4. 2D materials for 1D fiber supercapacitors

SCs offer high power density, fast charge/discharge rates, long cycling life.[17] FSCs with the 1D cylindrically shaped structure provide additional mechanical flexibility, which is promising for wearable devices.[10] Depending on their different energy storage mechanisms, electrode materials are required to provide high EDLC or pseudocapacitance. Various 2D materials are being explored as electrode materials to create high-performance FSCs. In the following five sub-sessions, we summarize recent studies of different types of 2D materials, including graphene-family materials, TMDs, TMOs/TMHs, and MXenes, respectively.

4.1. Graphene-family materials

Graphene-family materials include graphene, GO and reduced GO (rGO). Fig. 3 illustrates their structural differences. Graphene is a single layer of carbon atoms arranged in the covalent bonded hexagonal lattice. It has a large specific surface area (~2630 $m^2 g^{-1}$), a high Young's modulus (~1 TPa), and high electron mobility at room temperature (~10000 $cm^2 V^{-1} s^{-1}$).[43] The theoretical electrical double layer capacitance of graphene is ~550 F g^{-1}.[44] GO is obtained by chemical oxidation and exfoliation of graphite.[45, 46] Comparing to graphene, GO possesses a large amount of oxygen-containing functional groups, such as carboxyl groups localized mainly at its edge and hydroxyl and epoxy groups at its basal plane. Oxygen-containing functional groups improve its wettability and introduce additional pseudocapacitance. However, GO loses the high electrical conductivity of graphene. RGO is chemically reduced from GO by removing most of its surface functional groups and partially restoring the π-network of its basal plane, which results in much higher electrical conductivity than that of GO.[47] The graphene-family materials form a versatile material toolbox to fabricate fiber electrodes for FSCs. Table 1 summaries the properties of various FSCs fabricated using graphene-family material-based fiber electrodes. Other than discussing the details of the individual studies one by one, here we summarize key representative methods used in these studies and their critical issues.

There are several approaches to assemble nanoscale/macroscale graphene-family materials into macroscopic fibers, including wet-spinning,[48, 49] hydrothermal assembly,[50-52] and rolling of solid thin films.[53] These methods often start with a well-dispersed liquid suspension of GO. GO is subsequently self-assembled into desirable fiber structures and reduced to rGO. The fiber formation mechanisms of these methods have been comprehensively reviewed previously.[54] Their specific surface area, electrical conductivity, and mechanical properties are critical for the performance of fiber electrodes. A large

electrolyte ion accessible specific surface area offers high EDLC; high electrical conductivity allows fast electron transfer to enable good performance at fast charging and discharging rates, and good mechanical properties are required for fabricating flexible devices. It should be noted that besides serving as building blocks of freestanding fiber electrodes, graphene-family materials also act as mechanical supports, conductive enhancers or stress buffers in composite fibers assembled with other 2D materials, which are discussed in later sections focusing on 2D materials. In this section, we focus on how to improve the specific surface area, electrical conductivity, and mechanical properties of FSC electrodes assembled using graphene-family materials.

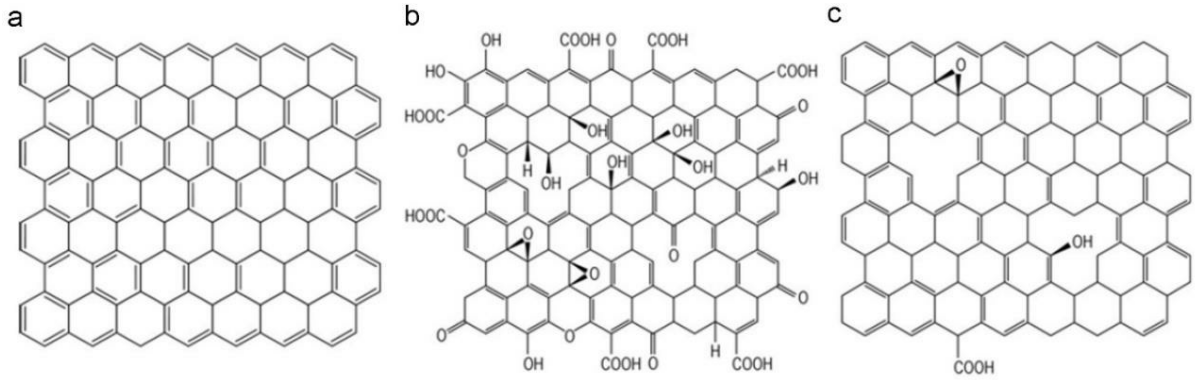

Fig. 3. Graphene-family materials: (a) graphene, (b) GO, and (c) rGO.

The specific surface area of pristine graphene fibers (*i.e.,* rGO fibers) is usually much smaller than that of graphene due to the severe re-stacking of rGO nanosheets caused by strong π-π interactions, which significantly compromise the energy storage capacity of rGO fiber electrodes in FSCs. For example, the hydrothermally assembled rGO fibers reported by Yu *et al.* have a specific surface area of 24 m^2 g^{-1},[55] and the wet-spun rGO fibers have an even smaller specific surface area of ~11 m^2 g^{-1}.[56] Several approaches have been explored to prevent the stacking of rGO nanosheets and partially restore their high specific surface area. The first approach is to introduce nanoscale spacers among rGO nanosheets, such as CNTs

(see Fig. 4a), cellulose nanocrystals (CNCs) (see Fig. 4b), and metal oxide nanoparticles.[56-59] The highest specific surface area reported so far for spacer-intercalated rGO fibers is 398 m^2 g^{-1} by using single-walled carbon nanotubes (SWCNTs) as a spacer.[55] Alternatively, nanosized holes are introduced to GO nanosheets to form holey GO (HGO). HGO nanosheets can improve the pore connection, avoid dead space, and serve as shortcuts for electrolyte ion diffusion (see Fig. 4c).[60, 61] Duan *et al.* reported that the freeze-dried reduced HGO hydrogel has a specific surface area of ~ 430 m^2 g^{-1}, which is more than 2 times higher than that of freeze-dried rGO hydrogel at ~ 180 m^2 g^{-1}.[60] Top-down approaches can also create rGO fibers containing holey graphene nanosheets. For example, a wet-spun GO fiber was dipped into H_3PO_4 solution followed by calcination at 650 ℃ (see Fig. 4d), which created nanosized holes on graphene nanosheets and increase its specific surface area to 107 m^2 g^{-1}.[62] Loosely packed porous rGO fibers can be created by using suitable dispersion and coagulation solvents in wet-spinning to prevent the stacking of rGO nanosheets. For example, Wallace *et al.* used acidic GO dispersion together with an acetone coagulation bath to produced porous rGO fibers with an ultrahigh specific surface area of 2210 m^2 g^{-1} (Fig. 4e).[63]

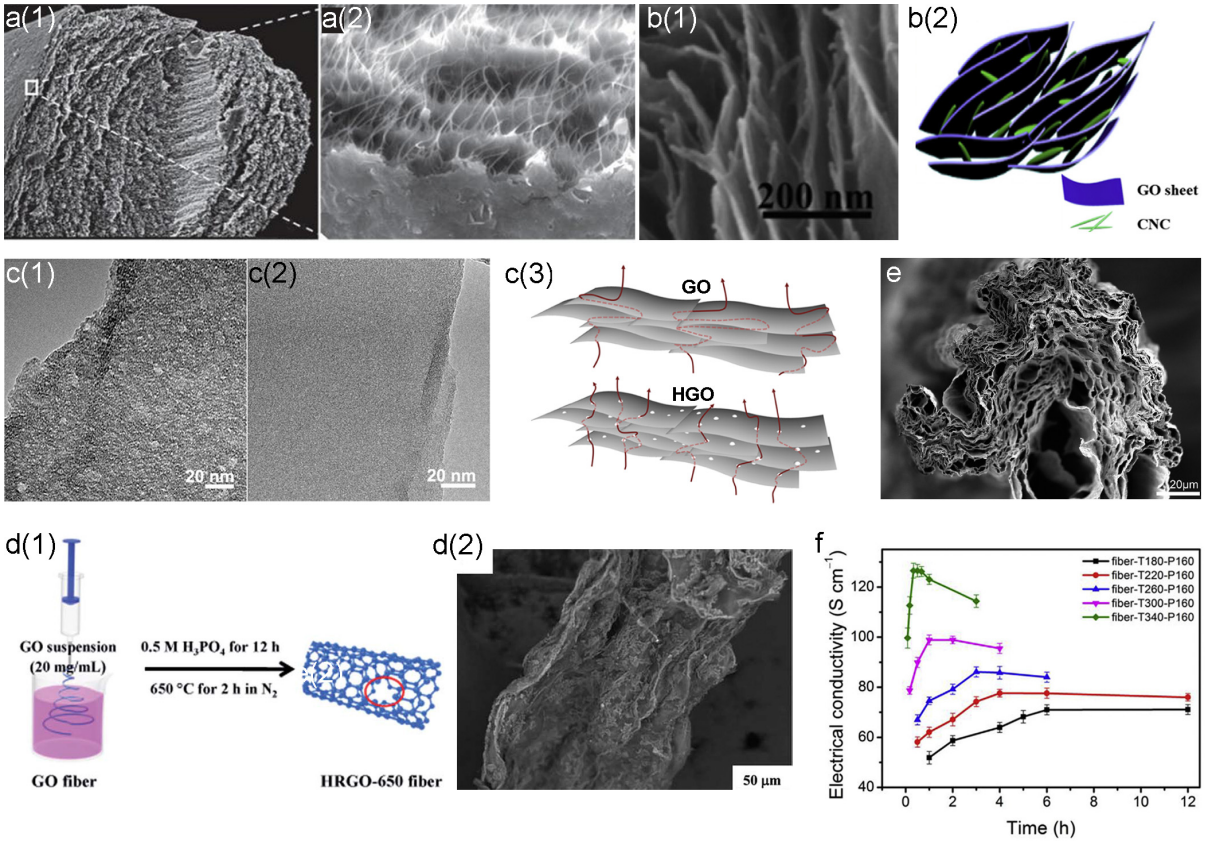

Fig. 4. (a) SEM images of the cross-section of an rGO/SWCNT hybrid fiber. Reproduced with permission.[55] Copyright 2014, Springer Nature. (b1) An SEM image and (b2) the corresponding schematic illustration of the cross-section of an rGO/CNC hybrid fiber. Reproduced with permission.[56] Copyright 2017, Elsevier. (c1) TEM images of an HGO nanosheet and (c2) a non-holey GO nanosheet. (c3) Schematic illustration of the electrolyte ion diffusion across graphene hydrogels assembled using HGO and GO nanosheets. Reproduced with permission.[60] Copyright 2015, American Chemical Society (ACS). (d1) Schematic illustration of a top-down approach for assembling rGO fibers comprised of holey graphene nanosheets and (d2) an SEM image of the fiber. Reproduced with permission.[62] Copyright 2016, RSC. (e) An SEM image of the cross-section of a wet-spun porous rGO fiber. Reproduced with permission.[63] Copyright 2014, ACS.

Pristine graphene has excellent electrical conductivity due to its perfect long-range-conjugated graphitic network. Graphene fibers are usually formed by assembling GO nanosheets, followed by reducing GO into rGO. The reduction sometimes is carried out simultaneously with assembly, for example in hydrothermal assembly methods. The lattice defects in graphitic basal planes and the remaining surface functional groups (*e.g.,* hydroxyl, carboxyl) in rGO nanosheets significantly interrupt the electron transfer in graphitic networks. Furthermore, large contact resistances exist among individual rGO nanosheets. Thus, the electrical conductivity of rGO fibers is often unsatisfactory for FSCs. Currently, four approaches are being explored to increase their electrical conductivity: tailoring the properties of starting materials (*i.e.,* GO nanosheets), doping GO/rGO nanosheets with heteroatoms, optimizing the reduction and assembly conditions, and forming hybrid fibers with more conductive materials. Depending on preparation methods, the C/O ratio of GO nanosheets typically ranges from 1:1 to 4:1.[64] After reduction, the C/O ratio in rGO nanosheets can reach about 8:1 to 15:1.[54, 64] RGO fibers assembled using GO nanosheets with fewer lattice defects and surface functional groups are expected to have higher electrical conductivity. Besides, larger GO nanosheets may minimize the contact junctions among rGO nanosheets in rGO fibers, which helps to decrease the contact resistance, yielding higher electrical conductivity.[49, 63] Recent studies have reported some new electrochemical exfoliation based methods,[65, 66] for producing high-quality GO nanosheets with fewer defects. They may be used to assemble rGO fibers with higher electrical conductivity. Doping graphene materials with heteroatoms often significantly changes their electrical conductivity.[67] B, N, P, and S doped or their co-doped GO/rGO have shown better electrical conductivity than pristine GO/rGO, which also introduce additional pseudocapacitance.[67, 68] For example, 2.8 at.% N doping in rGO/SWCNT fibers increases the volumetric capacitance over 50% to 305 F cm^{-3}.[55] The reduction of rGO fibers can be

carried out by chemical reduction via various reducing agents, high-temperature treatment in inert gas, hydrothermal treatment, or the combination of these methods. Stronger reducing agents or higher calcination temperature often lead to higher degree of reduction, which is beneficial to improve electrical conductivity.[64] Our recent study also shows that rGO fibers can be reduced more extensively and faster in near-critical water at a higher hydrothermal temperature (Fig. 4f).[51] On the other aspect, CNTs are the most often used conductive materials to increase the electronic conductivity of rGO fibers, the electrical conductivity of rGO/CNT hybrid fibers can reach about 5 to 9 times higher than that of rGO fibers.[55, 69] Conducive metal oxides (*e.g.,* RuO_2)[50] and conductive polymers[52] have also been used to enhance the electrical conductivity of rGO fibers.

Mechanical properties of graphene fibers depend on the alignment, compactness, and cross-link among adjacent rGO nanosheets as well as the intrinsic properties of GO nanosheets. For example, GO nanosheets with larger lateral size reduce the junctions among rGO nanosheets in rGO fibers, resulting in better mechanical properties.[49, 63] Usually, rGO nanosheets with less functional groups and defects create better alignment and higher densification in assembled rGO fibers, leading to improved tensile strength.[49] However, entirely removing functional groups and defects in rGO nanosheets has negative impacts on their mechanical properties. For example, Lian *et al.* found that rGO fibers have the optimum tensile strength of ~ 800 MPa after annealed at 1800 C^o. Further increasing the annealing temperature deteriorates their tensile strength because of the removing of the crosslinks among rGO nanosheets at the high annealing temperature.[49] Besides, the interactions among rGO nanosheets in rGO fibers are sensitive to the properties of GO dispersions, such as pH[63] and viscosity,[54] as well as their assembly conditions, such as coagulation baths used for wet-spinning.[63] Tailoring these parameters also strongly affects the mechanical properties of resulting rGO fibers. Alternatively, the tensile strength of rGO fibers may be

improved when interfacial spacers are introduced among rGO nanosheets. For example, Zhu *et al.* showed that rGO/CNC fibers have a higher tensile strength of 199.8 MPa compared to that of pristine rGO fibers at 157.5 MPa because of the formation of hydrogen bonds among hydroxyl groups between CNCs and rGO nanosheets.[56] Similar phenomenon was also observed in rGO/few-walled CNT hybrid fibers. The hybrid fiber possesses a much higher tensile strength of 385.7 MPa than that of pristine rGO fibers at 193.3 MPa.[69] However, not all spacers can improve the tensile strength of composite fibers. For example, acid-functionalized single-walled CNTs were found to weaken the tensile strength of rGO fibers.[55] Furthermore, many polymers have been explored to reinforce rGO fibers.[70, 71] However, some polymers could block the transport channels of electrolyte ions in rGO fibers, leading to poor energy storage performance.

We have discussed different approaches to improve the specific surface area, electrical conductivity, and mechanical properties of graphene fibers. Nevertheless, these approaches sometimes create contradictory effects. For example, HGO is beneficial for increasing the specific surface area, on the other hand, the nanopores in HGO sheets destroy long-range-conjugated graphitic networks, leading to lower electrical conductivity. The removal of surface functional groups on rGO nanosheets is favorable for improving both the electrical conductivity and the tensile strength. But, hydrophobic rGO nanosheets reduce the wettability of fiber electrodes in electrolytes. Thus, it is important to carefully consider the trade-offs of these approaches to yield fiber electrodes with desirable properties.

Table 1. Physiochemical properties of GO dispersions and the corresponding assembled rGO fibers, their assembly conditions, and the electrochemical performances of rGO fibers. (SSA: specific surface area; HT: hydrothermal; WS: wet-spinning; NLCS: non-liquid-crystal spinning; NA: not available; PVA: polyvinyl alcohol)

Fibers	**GO**			**Assembly method**	**Reduction method**	**C / O**	**Electrical conductivity (S cm^{-1})**	**Tensile strength (MPa)**	**Diameter (μm)**	**Density (g cm^{-3})**	**SSA (m^2 g^{-1})**	**Electrolyte**	**Capacitance**	**ref.**
	Size (μm)	**C / O**	**pH**											
rGO	2.5	NA	NA	HT	HT at 220℃	NA	12	197	40	0.29	24	1M H_2SO_4	~ 90 F cm^{-3} at ~ 70 mA cm^{-3}	[55]
												PVA/H_3PO_4	NA	
N-rGO/ CNT (1:1)	2.5	NA	NA	HT	HT at 220 ℃	NA	102	84	60	0.59	396	1M H_2SO_4	305 F cm^{-3} at ~ 73.5 mA cm^{-3}	[55]
												PVA/H_3PO_4	300 F cm^{-3} at ~ 26.7 mA cm^{-3}	
N-rGO/ CNT (1:1)	NA	NA	NA	HT	HT at 180 ℃	5.7	71	NA	72	0.85	391	1M H_2SO_4	243 F cm^{-3} at 2 mV s^{-1}	[51]

N-rGO/ CNT (1:1)	NA	NA	NA	HT	HT at 340 ℃	11.1	127.5	NA	60	1.13	387	1M H_2SO_4 PVA/H_3PO_4	322 F cm^{-3} at 2 mV s^{-1} 308 F cm^{-3} at 2 mV s^{-1}	[51]
rGO	40	NA	NA	HT	HT at 180 ℃	NA	7.8	180.5	42	0.68	NA	PVA/H_3PO_4	~ 120 F cm^{-3} at 72.2 mA cm^{-3}	[72]
N-rGO/ MWCNT (4:1)	40	NA	NA	HT	HT at 180 ℃	NA	31.6	153.7	48	0.98	NA	PVA/H_3PO_4	252 F cm^{-3} at 2mV s^{-1}	[72]
rGO	>50	0.33	3	WS (acetone as coagulation bath)	Annealing at 220 ℃ under vacuum	0.89	25.1	10.13	NA	NA	2210	1M H_2SO_4 (2-electrode)	409 F g^{-1}	[63]
rGO	0.5-1	NA	NA	NLCS	HI	NA	71.9	157.5	Cal. ~ 33	0.14	11	1M H_2SO_4	~ 18 F g^{-1} at 2 mV s^{-1}	[56]
rGO/ CNC (5:1)	0.5-1	NA	NA	NLCS	HI	NA	64.7	199.8	Cal. ~ 33	0.15	24	1M H_2SO_4	141.1 F g^{-1} at 2 mV s^{-1}	[56]
rGO	0.212	2.44	11	NLCS	HI	7.14	15.3	208	~ 200	NA	231	1M H_2SO_4	~ 245 F g^{-1} at 0.25 A g^{-1}	[54]
rGO	~ 23	NA	NA	WS	Annealing at 1800 ℃	NA	~ 800	~ 800	NA	1.45	NA	NA	NA	[49]

rGO	0.8 (30%) & ~ 23 (70%)	NA	NA	WS	Annealing at 1800 ℃	NA	1110	1080	NA	1.75	NA	NA	NA	[49]
rGO	NA	NA	NA	other	Vitamin C	NA	42	~ 400	101	NA	40.6	PVA/H_3PO_4	212.9 mF cm^{-2}	[73]
Hollow rGO/ PEDO: PSS	NA	NA	NA	other	Vitamin C	NA	47	631	77	NA	71	PVA/H_3PO_4	304.5 mF cm^{-2}	[73]
rGO	NA	NA	NA	WS	Laser	NA	NA	NA	50	NA	NA	[EMIM][BF4]	1.2 mF cm^{-2} at 80 μA cm^{-2}	[74]
rGO (core-sheath)	NA	NA	NA	HT	HT at 220 ℃	NA	10–20	~ 150	30	0.23	NA	PVA/H_2SO_4	1.2-1.7 mF cm^{-2} (device)	[75]
rGO	NA	NA	NA	WS	HI	NA	60	NA	10–100	NA	NA	1 M H_2SO_4	204.8 mF cm^{-2} at 10 mV s^{-1}	[76]
rGO	NA	NA	7	HT	Vitamin C + HT at 180 ℃	NA	NA	90	100	NA	NA	1 M H_2SO_4	61.4 F g^{-1} at 10 mV s^{-1}	[77]
rGO/ PANI	NA	NA	7	HT	Vitamin C + HT at 180 ℃	NA	NA	140	105	NA	NA	1 M H_2SO_4	193.65 F g^{-1} at 10 mV s^{-1}	[77]

rGO	50	NA	NA	WS	HI	NA	53.5	193.3	20	0.81	NA	PVA/H_3PO_4	38.8 F cm^{-3} at 50 mA cm^{-3} (device)	[69]
rGO/ few-walled CNT	50	NA	NA	WS	HI	NA	210.7	385.7	24	1.08	NA	PVA/H_3PO_4	23.58 F cm^{-3} (device)	[69]
rGO	NA	NA	NA	WS	Annealing at 650 ℃	NA	NA	NA	110	NA	107	1M Na_2SO_4	49 F g^{-1} at 1 A g^{-1}	[62]

4.2. Transition metal dichalcogenides

TMD monolayers are atomically thin 2D semiconductors in the form of MX_2, where M is a transition metal from group 4–10 (*e.g.*, Mo or W) and X is a chalcogen (e.g., S, Se, or Te).[34] One transition metal atomic layer is sandwiched between two layers of chalcogen atoms. Covalent bonds exist in individual layers and van der Waals forces dominate between layers. TMD monolayers can provide large exposed surface and abundant surface sites for electrostatic adsorption or surface redox reactions. Besides, some TMDs have multiple phases with diverse electrical properties, ranging from insulating, semiconducting to metallic.[27] These unique properties have attracted interests of using them for capacitive energy storage applications.

Among various TMD materials, MoS_2 is currently the most popular electrode materials for SCs due to its high specific capacitance (~ 1000 F g^{-1}).[78, 79] Several recent studies have incorporated 2D MoS_2 layers into CNT or rGO fibers to fabricate FSCs. For example, Peng *et al.* designed aligned CNT/MoS_2 hybrid fibers by hydrothermally grown few-layered MoS_2 nanosheets on CNT sheets, followed by twisting the CNT/MoS_2 hybrid sheets into fibers (see Fig. 5a).[76] The resulting hybrid fibers have a high MoS_2 mass loading of 86 wt.%. Two PVA/H_3PO_4 gel coated CNT/MoS_2 hybrid fibers were twisted together to form a solid-state FSC, delivering a volumetric capacitance of 135 F cm^{-3} at the CV (cyclic voltammetry) scan rate of 5 mV s^{-1}. Alternatively, Chen *et al.* drop-casted a single-layer MoS_2-GO mixture on multi-walled carbon nanotube (MWCNT) sheets and then twisted them into fibers followed by reduction using HI (see Fig. 5b).[80] The rGO nanosheets were found to improve the interaction between MoS_2 and MWCNTs. The solid-state FSC fabricated using the hybrid fibers with a MoS_2 mass loading of 6.3 wt.% delivers a volumetric capacitance of 4.8 F cm^{-3} at 0.5 F cm^{-3}. Peng *et al.* also demonstrated a one-step hydrothermal method to prepare rGO/MoS_2 hybrid fibers with a MoS_2 mass loading of 23.03 wt.% (see Fig. 5c).[81] The

resulting solid-state FSC achieved a volumetric capacitance of ~ 130 F cm^{-3} at the current density of 0.1 A cm^{-3}. Furthermore, Chen *et al.* have synthesized several TMD monolayers via electrochemical exfoliation, including MoS_2, TiS_2, TaS_2, and $NbSe_2$. The corresponding rGO/TMD hybrid fibers were assembled by a wet-spinning method.[82] Considering the electrical conductivity of metal wires is several orders higher than that of carbon material-based fibers, several studies deposited TMD monolayers on the surface of metal wires to create fiber electrodes for FSCs. For example, Wang *et al.* synthesized Ti/TiO_2/MoS_2 coaxial fibers by hydrothermally growing MoS_2 nanosheets on Ti wires with a TiO_2 buffer layer (see Fig. 5d).[73] The TiO_2 layer was found to improve the adhesion between MoS_2 nanosheets and Ti wires. The resulting solid-state FSC deliver a specific volumetric capacitance of 70.6 F cm^{-3}.

Most of MoS_2-based FSCs have used the thermodynamically stable 2H phase of MoS_2, which is semiconducting with poor electrical conductivity. In contrast, the 1T phase of MoS_2 is metallic, and the electrical conductivity is 10^7 times higher than that of the 2H phase. Besides, the 1T phase of MoS_2 has an enlarged interlayer spacing, containing much more electrochemically active sites, and its surface is also more hydrophilic (see Fig. 5e).[33, 83] Chhowalla *et al.* reported that a 1T phase MoS_2 film can deliver a specific capacitance ranging from ~ 400 to 700 F cm^{-3} in a variety of aqueous electrolytes (see Fig. 5e).[83] Veerasubramani *et al.* prepared some few-layered 1T MoS_2 from bulk MoS_2 by ball-milling and then brush-coated the 1T MoS_2 on stainless steel wires. Afterward, two MoS_2/stainless steel wire composite electrodes were placed in parallel and sandwiched in PVA/LiCl gel electrolyte in a flexible tube. The resulting FSCs delivered a specific capacitance of 119 μF cm^{-1} and an energy density of 8.1 nWh cm^{-1}, and they can keep ~ 90 % capacitance when the charge/discharge current increases from 2.5 to 25 μA (Fig. 5f).[84]

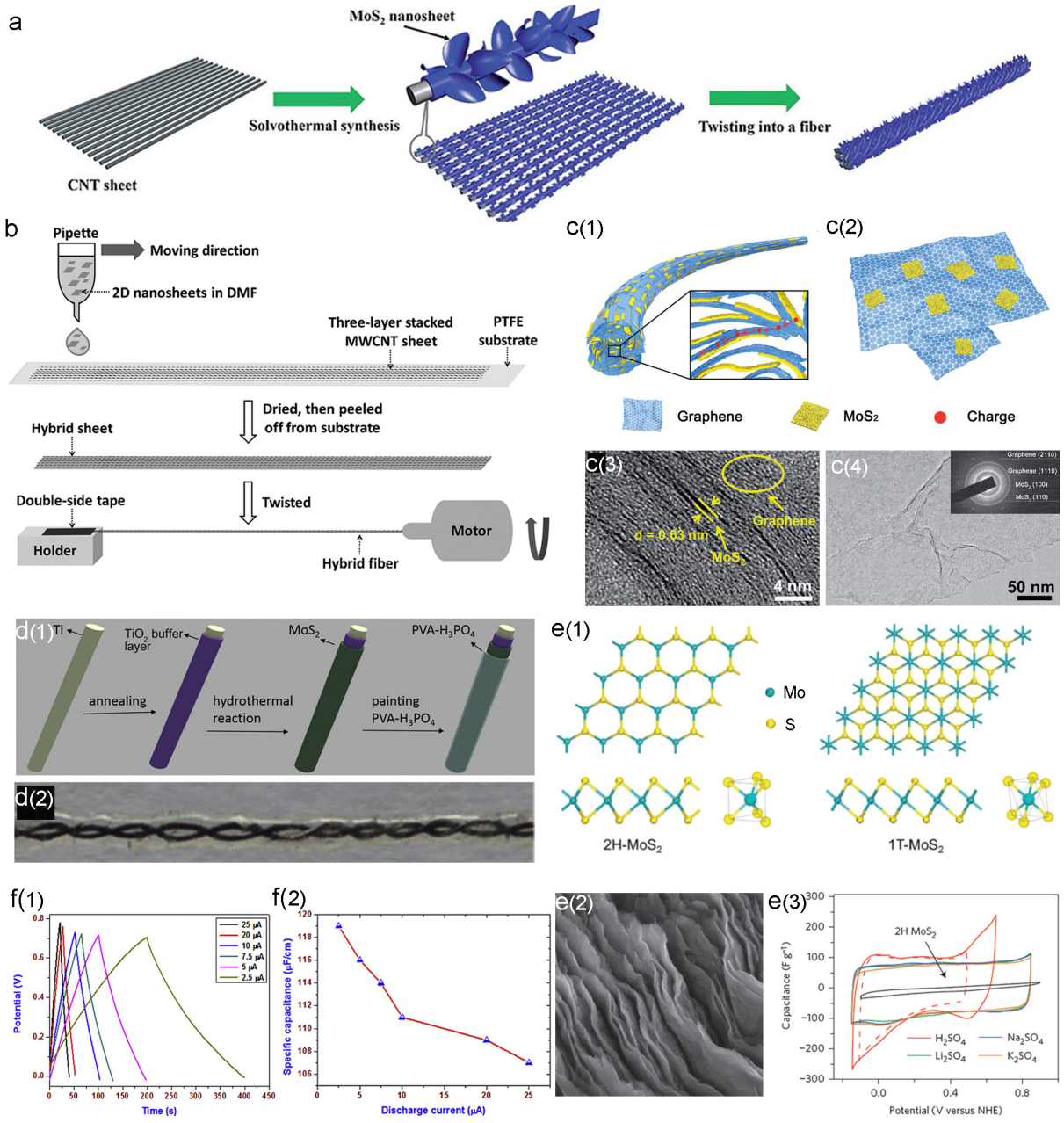

Fig. 5. (a, b) Schematic illustration of the synthesis of CNT/MoS_2 hybrid fibers. Reproduced with permission.[76, 80] Copyright 2015, Wiley-VCH. Copyright 2015, RSC. (c1) Schematic illustration of the structure of a graphene/MoS_2 hybrid fiber and (c2) the epitaxial growth of MoS_2 sheets on graphene. (c3, c4) TEM images of the graphene/MoS_2 hybrid fiber. Reproduced with permission.[81] Copyright 2017, RSC. (d1) Schematic illumination of the synthesis of a Ti/TiO_2/MoS_2 electrode coated with electrolytes. (d2) A photo of FSC made of twisted Ti/TiO2/MoS_2 electrodes. Reproduced with permission.[73] Copyright 2015, Elsevier.

(e1) Top and side views of the atomic structures of 2H and 1T phases of MoS_2 monolayers. Reproduced with permission.[85] Copyright 2015, ACS. (e2) an SEM image of a film electrode fabricated using 1T phase MoS_2 nanosheets by vacuum filtration. (e3) CV curves of the film in 0.5 M sulfate electrolyte at the scan rate of 20 mV s^{-1}. Reproduced with permission.[83] Copyright 2015, Springer Nature. (f1) GCD (galvanostatic charge/discharge) curves of an FSC based on 1T phase MoS_2 measured at different currents (2.5–25 mA) and (f2) the correlation between the specific capacitance and the discharge current. Reproduced with permission.[84] Copyright 2016 Elsevier.

4.3. Transition metal oxides/metal hydroxides

Some TMOs/TMHs are intrinsic pseudocapacitive materials, such as RuO_2 and MnO_2. SCs based on these materials are characterized by a linear sweep rate (v) dependence on the current ($i \sim v$) in cyclic voltammetry (CV) tests. In contrast, many other TMOs/TMHs are transitional battery materials, such as NiO and $Ni(OH)_2$. Charging/discharging energy storage devices based on these materials in bulk involves phase transformations and exhibit classic semi-infinite diffusion behavior ($i \sim v^{0.5}$), and they should be considered as batteries other than SCs. However, when the dimensions of battery materials are reduced to nanometer scale (*e.g.,* existing as 2D nanosheets), faradic reactions would mostly take place on their surfaces with reduced diffusion limits. Thus, they may demonstrate high extrinsic pseudocapacitance.[79, 86] For example, 2D NiO nanosheets show the high specific capacitance of 3750 F g^{-1}.[87] The challenges of applying 2D TMOs/TMHs in FSCs originates from their poor electrical conductivity and structural stability upon phase transformations. FSCs based on 2D TMOs/TMHs often suffer from poor rate capability and cycling stability. Current research studies of 2D TMOs/TMHs for FSCs focus on tailoring the

structure 2D TMOs/TMHs to address these challenges. The research efforts on several types of 2D TMOs/TMHs, including MnO_2, Co_3O_4, $NiO/Ni(OH)_2$ and several others, are described in the following sub-sessions.

4.3.1. MnO_2

MnO_2 is the most frequently reported pseudocapacitive materials for FSCs due to its high specific capacitance (~ 1380 F g^{-1}), low cost, and environmental friendliness.[88] MnO_2 has multiple crystalline structures, including amorphous, α-, β-, γ- and δ-. α-, β-, γ-MnO_2 have a tunneled structure, and α-MnO_2 has relatively larger tunnels. δ-MnO_2 has a relatively open layered structure. Thus, amorphous MnO_2, α-MnO_2, and δ-MnO_2 are more often used in FSCs because their open structures facilitate the mass transfer of electrolyte ions.[17]

Zhou *et al.* reported the earliest study on MnO_2-based FSCs in 2012, in which MnO_2 nanoparticles were deposited on carbon fiber (CF) via a redox reaction with $KMnO_4$ (illustrated in Fig. 6a).[89] A solid-state FSC was fabricated using the MnO_2/CFs core-sheath fiber electrodes in PVA/H_3PO_4 gel electrolytes, exhibiting a volumetric capacitance of 2.5 F cm^{-3}, an energy density of 0.22 mW h cm^{-3} at the power density of 0.4 mW cm^{-3}. However, using the redox reaction of $KMnO_4$ to synthesize MnO_2 is difficult to avoid the agglomeration of MnO_2 nanoparticles. Large MnO_2 particles limit the mass transfer of electrolyte ions, resulting in poor energy storage performance.[90] Thus, considerable research efforts have been devoted to synthesizing MnO_2 2D structures, including 2D nanosheets, nanoflakes, and flower-like nanoplates. It has been proposed that those 2D structures can lower ionic resistance with shorter transport path, offer larger accessible surface area, and provide efficient electron transfer due to higher electrical conductivity. Zhang *et al.* directly electrodeposited ultrathin 2D MnO_2 nanosheets on CF yarns, and two

resulting MnO_2/CF electrodes were placed in parallel and separated by PVA/Na_2SO_4 gel electrolyte (Fig. 6b).[91] The assembled FSCs exhibited a volumetric energy density of 3.8 mW h cm^{-3} at a power density of 89 mW cm^{-3}. Zhu *et al.* grew ultrathin MnO_2 nanosheets with 5–7 layers on CFs via a hydrothermal method (see Fig. 6c). A solid-state, asymmetric FSC was assembled using the MnO_2/CF electrode as the positive electrode and rGO on CFs as the negative electrode, displaying an energy density of 27.2 Wh kg^{-1} at the power density of 979.7 W kg^{-1}.[92]

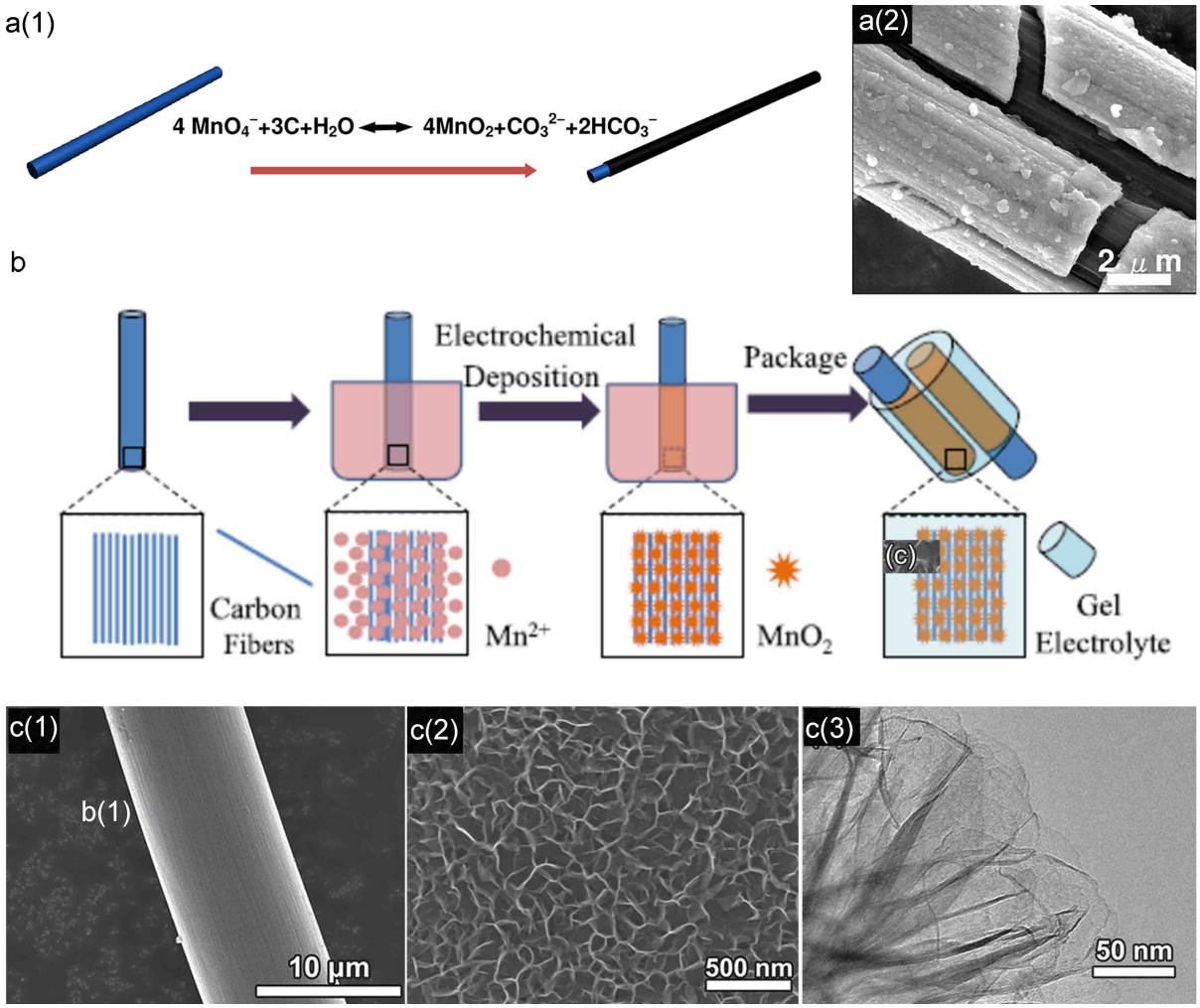

Fig. 6. (a1) Schematic illustration of the synthesis of a MnO_2/CF core-shell fiber, and (a2) an SEM image of the fiber. Reproduced with permission.[89] Copyright 2012, ACS. (b) Schematic illustration of the fabrication of MnO_2/CF-based flexible solid-state FSCs. Reproduced with permission.[91] Copyright 2016, Elsevier. (c1 and c2) SEM images of

MnO_2 nanosheet arrays on a CF, and a TEM image of MnO_2 nanosheets (c3). Reproduced with permission.[92] Copyright 2015, Wiley-VCH.

In general, the surface area of pristine CFs or metal wires is too small to accommodate a high mass loading of MnO_2. For example, the specific surface area of common CFs is less than 10 $m^2\ g^{-1}$. Thus, several approaches have been explored to increase the mass loading of MnO_2 in fiber electrodes. First, rGO has been used as interfacial binders, which provides large surface area and many reactive surface sites for anchoring MnO_2. Further, rGO has a high electrical conductivity, which provides excellent interfacial contact between MnO_2 and substrates for enabling efficient electron transport. Besides, porous rGO composites may also facilitate the mass transfer of electrolyte ions.[93, 94] For example, Wang *et al.* assembled an asymmetric FSC using the MnO_2/rGO/CF fiber as the positive electrode and the rGO/CF fiber as the negative electrode, which can be operated up to 1.6 V, and exhibit a high volumetric energy density of 1.23 mW h cm^{-3} at the power density of 0.27 W cm^{-3} (see Fig. 7a).[93] Second, 1D nanowires (NWs) have been used as interfacial binders.[95, 96] For example, Zhang *et al.* synthesized ZnO NW arrays on CNT fibers and then deposited MnO_2 on these ZnO NWs to form MnO_2/ZnO/CNT composite fibers (see Fig. 7b).[96] Third, holey rGO fibers with a large specific surface area have been used as substrates to form MnO_2/holey rGO composite fibers. Pristine rGO fibers have a limited specific surface area (~ 24 $m^2\ g^{-1}$).[55] Liu *et al.* dipped GO fibers in H_3PO_4 solution and then calcined them at 650 ℃ to create holey rGO fibers with a specific surface area of 107 $m^2\ g^{-1}$ (see Fig. 4d). [62] An FSC was assembled by intertwined two MnO_2/holey rGO fiber electrodes, which shows an areal capacitance of 16.7 mF cm^{-2}.

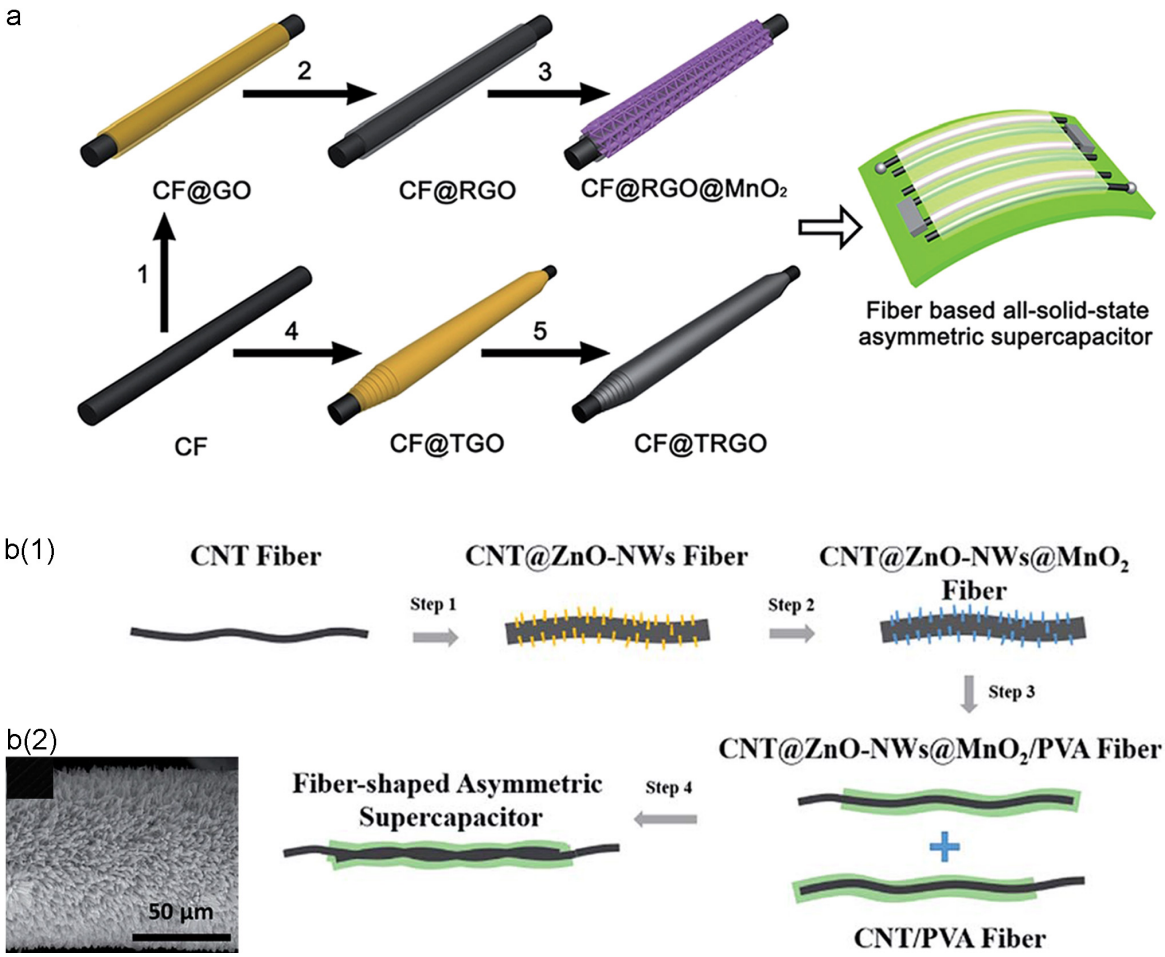

Fig. 7. (a) Schematic illustration of the assembly of an asymmetric FSC based MnO_2/rGO/CF and rGO/CF fiber electrodes. Reproduced with permission.[93] Copyright 2015, RSC. (b1) Schematic illustration of the fabrication of an asymmetric FSC based on MnO_2/ZnO/CNT and CNT fiber electrodes. (b2) An SEM image of the MnO_2/ZnO/CNT composite fiber. Reproduced with permission.[96] Copyright 2016, RSC.

The poor electrical conductivity of MnO_2 often dramatically depresses its energy storage capacity, especially at high charging/discharging rates. Coating MnO_2 with a conductive polymer layer has been used to address this issue, and some conductive polymers can also contribute some additional pseudocapacitance. Further, conductive polymers may also serve as efficient binders to avoid the detachment of MnO_2 nanoparticles from fiber substrates.[35, 97] For example, Gao *et al.* designed hierarchical ternary polypyrrole (PPy)/MnO_2/CF fibers

by electrodepositing MnO_2 and PPy on CFs (see Fig. 8a).[98] An FSC assembled using these fiber electrodes exhibited a volumetric capacitance of 69.3 F cm^{-3}, an energy density of 6.16 mW h cm^{-3} at the power density of 40 mW cm^{-3}. Zhi *et al.* deposited rGO, MnO_2, and PPy on stainless steel yarns to create yarn electrodes.[99] The excellent mechanically strength of stainless steel yarns enable them to be knitted into cloth using a commercial cloth knitting machine (see Fig. 8b). Peng *et al.* prepared a ternary hybrid fiber by synthesizing MnO_2 nanosheets on CNT fibers coated with poly(3,4-ethylenedioxythiophene)-poly(styrenesulfonate) (PEDOT: PSS). An asymmetric FSC was assembled using a MoO_2/PEDOT: PSS/CNT fiber as the positive electrode and an ordered microporous carbon (OMC)/CNT fiber as the negative electrode, which delivered an energy density of 11.3 mWh cm^{-3} at the power density of 30 mW cm^{-3}.[97]

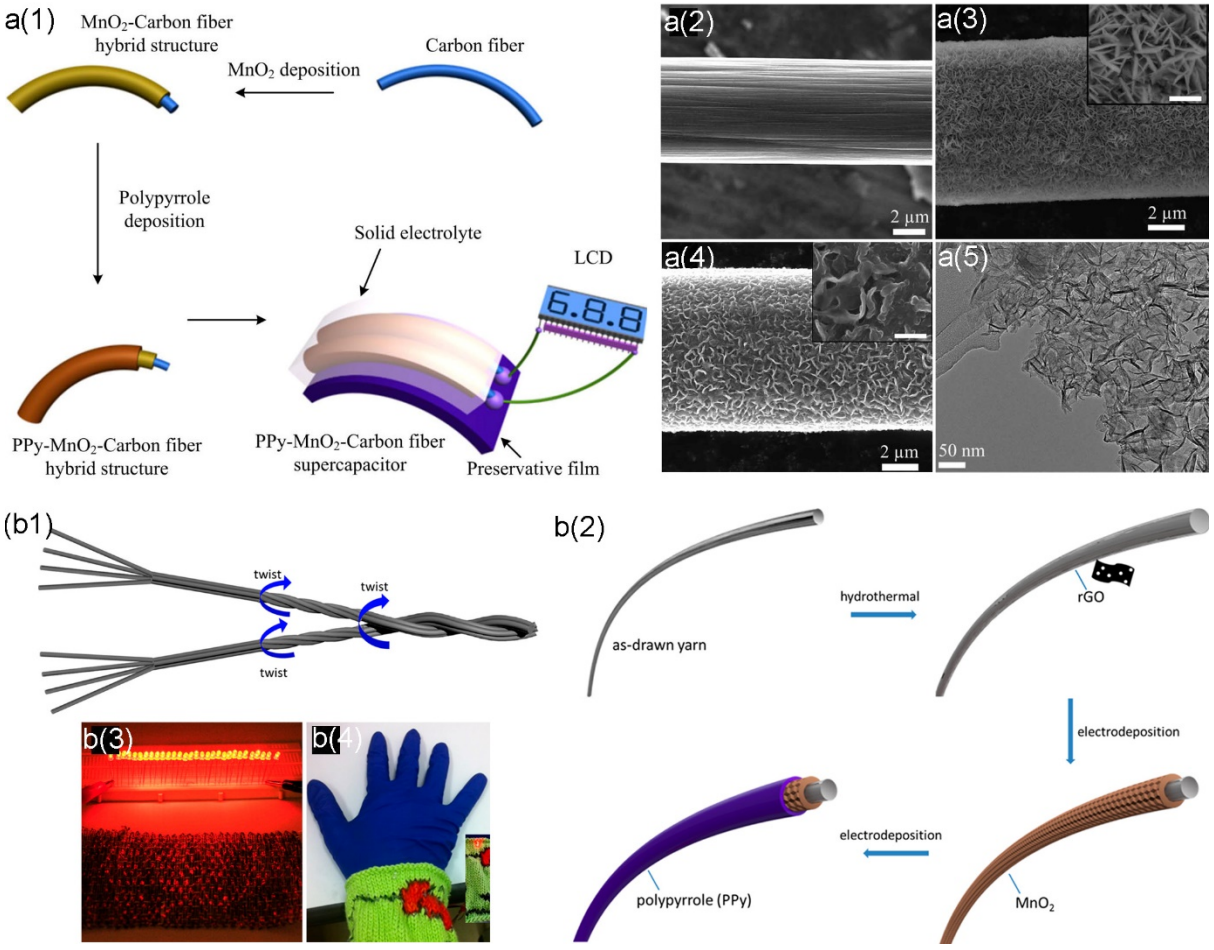

Fig. 8. (a1) Schematic illustration of the fabrication of an FSC based on PPy/MnO_2/CF fiber electrodes, (a2, a3, and a4) SEM images of the CF, MnO_2 nanoflakes deposited on the CF, PPy wrapping on the MnO_2/CF, respectively. (a5) A TEM image of MnO_2 nanoflakes. Reproduced with permission.[98] Copyright 2013, Springer Nature. (b1) Schematic illustration of the stainless-steel yarn twisting. (b2) Schematic illustration of the fabrication of the PPy/MnO_2/rGO/stainless-steel yarn electrodes. (b3 and b4)) Photographs of the energy storage textiles made of the yarns. Reproduced with permission.[99] Copyright 2015, ACS.

4.3.2. Co_3O_4

Co_3O_4 is another potential pseudocapacitive material due to its high theoretical specific capacitance of 3560 F g^{-1} and good redox reaction reversibility.[100] However, the high cost and toxicity are two critical drawbacks of Co_3O_4 as capacitive materials. Many studies have partially replaced Co in Co_3O_4 using cheaper and environment-friendly elements, such as Zn, Ni, Cu, and Fe. Some of these Co_3O_4 isostructures show superior capacitive performance resulting from their stronger electrochemical activity, richer redox reactions, and higher electrical conductivity. For example, $ZnCo_2O_4$, in which Zn^{2+} replaces Co^{2+} at tetrahedral sites in spinel Co_3O_4, has been found to be a high-performance pseudocapacitive material (see Fig. 9a).[101] In addition, Ni-doping has been found to significantly increase the electrical conductivity of Co_3O_4 from 3.1 × 10^{-5} S cm^{-1} to 0.1–0.3 S cm^{-1} for $Ni_xCo_{3-x}O_4$.[102] Jang *et al.* electrodeposited flower-like $NiCo_2O_4$ nanoflakes (with the thicknesses of ~ 20–30 nm) on a 3D porous Ni wire (Fig. 9b).[103] An FSC was assembled using the 3D porous fiber electrodes, which delivered a high capacitance of 30 F g^{-1} (3 F cm^{-3}) at the scan rate of 5 mV s^{-1}, an energy density of 2.18 W h kg^{-1} (0.21 mW h cm^{-3}), and

a power density of 21.6 W kg^{-1} (2.1 mW cm^{-3}). It retained 100% of its initial capacitance after 5000 charging/discharging cycles.

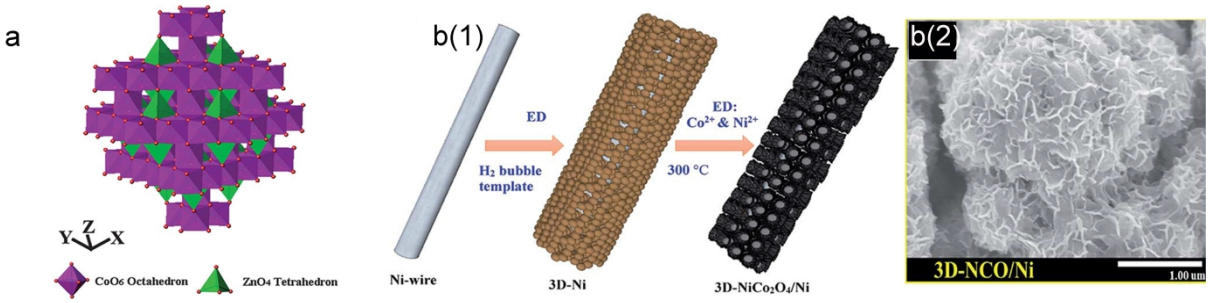

Fig. 9. (a) The crystal structure of spinel $ZnCo_2O_4$, in which Zn ions occupy tetrahedral sites, and Co ions occupy octahedral sites. Reproduced with permission.[101] Copyright 2012, RSC. (c1) Schematic illustration of the fabrication of a flexible coaxial FSC. (b1) Schematic illustration of the synthesis of 3D-NiCo2O4/Ni and its SEM image showing NiCo2O4 nanoflakes (b2). Reproduced with permission.[103] Copyright 2016, RSC

4.3.3. NiO/Ni(OH)$_2$

$NiO/Ni(OH)_2$ have attracted great interests as promising pseudocapacitive materials due to their high theoretical specific capacitance (> 3000 F g^{-1}), low cost and environmental friendliness, and simple synthesis methods.[17] A key issue of $NiO/Ni(OH)_2$ as a pseudocapacitive material is its low electrical conductivity. Several approaches have been explored to address this issue, including the formation of porous nanostructures, the formation of conductive composites, and the introduction of other metal ions in $NiO/Ni(OH)_2$.

First, highly porous 2D $NiO/Ni(OH)_2$ has been synthesized to shorten the electron and electrolyte ion transfer pathways, such as nanosheets, nanoflakes, nanoflowers and nanowalls. Second, $NiO/Ni(OH)_2$ has been hybridized with carbon materials or conductive polymers to form conductive composites. For example, Ma *et al.* synthesized $Ni(OH)_2$ nanosheets on

porous rGO coated Ni wires (see Fig. 10a).[104] An asymmetric FSC was assembled by coupling a $Ni(OH)_2$/rGO/Ni wire electrode with an rGO/Ni wire electrode, which delivered a specific volumetric energy density of 0.83 mW h cm^{-3} at the volumetric power density of 54 mW cm^{-3} and retained ~ 83% of its initial capacitance after 6000 charging/discharging cycles. Hu *et al.* encapsulated porous NiO/$Ni(OH)_2$ nanoflowers in 3D interconnected PEDOT on Cu-Ni wires.[105] An asymmetric FSC was assembled using this composite wire as a positive electrode and ordered mesoporous CFs as a negative electrode, delivering a specific energy density of 0.011 mW h cm^{-2} at the power density of 0.33 mW cm^{-2}. Third, Co ions have been introduced in NiO/$Ni(OH)_2$ to form Ni/Co double hydroxides, which not only increases the electrical conductivity but also create two types of active electrochemical sites, leading to superior energy storage performance compared with mono metal hydroxides.[94] For example, Lu *et al.* deposited Ni/Co double hydroxide nanosheets on Ni-coated CFs.[106] Subsequently, an asymmetric FSC was assembled using the Ni/Co double hydroxides/Ni/CFs as a positive electrode and pen ink deposited Ni-coated CFs as a negative electrode (see Fig. 10b), which exhibited a capacitance of 28.67 mF cm^{-2}, and an energy density of 9.57 μW h cm^{-2} at the power density of 492.17 μW cm^{-2}. It can retain 95.6% of its initial capacitance after 5000 charging/discharging cycles.

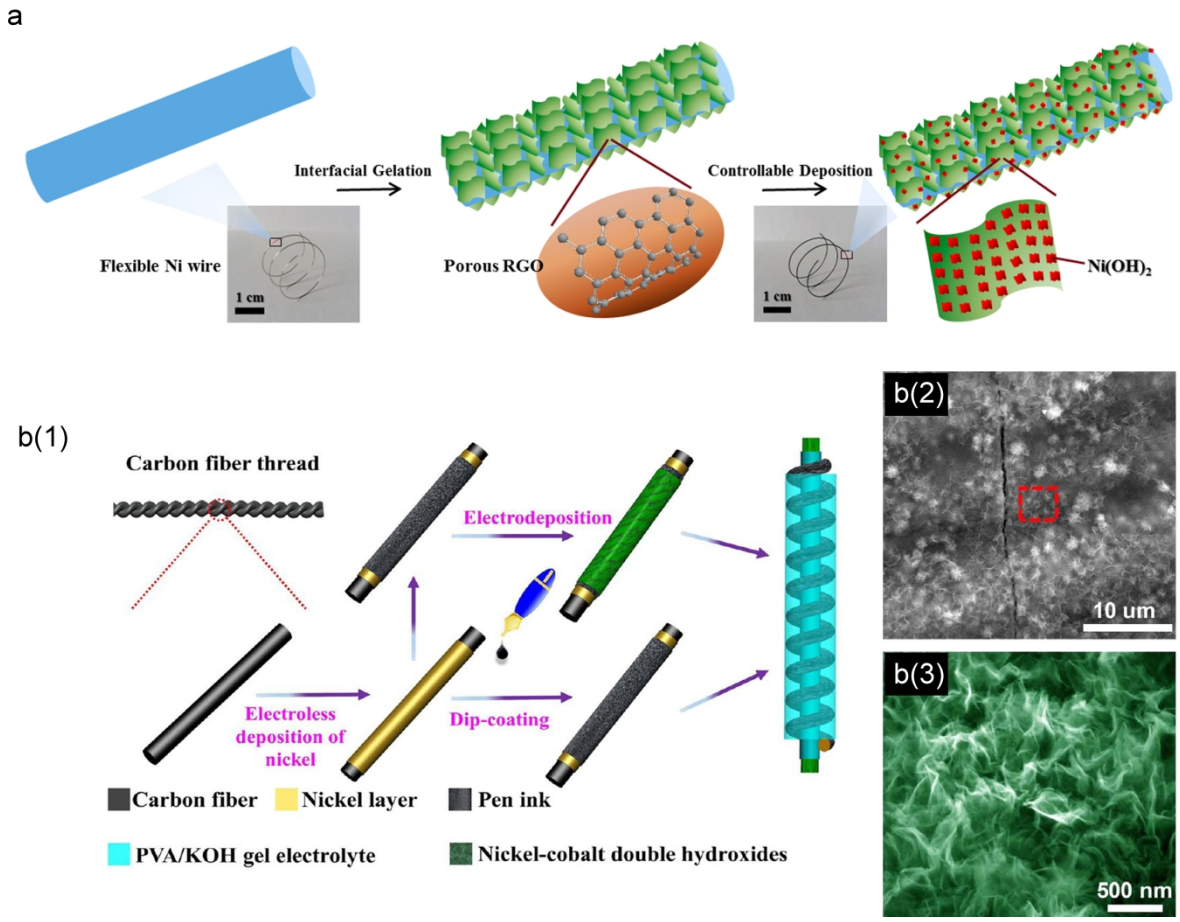

Fig. 10. (a) Schematic illustration of the synthesis of a $Ni(OH)_2$/rGO/Ni fiber electrode and insets are corresponding photos. Reproduced with permission.[104] Copyright 2016, ACS. (b1) Schematic illustration of the fabrication of a flexible asymmetric FSC using a Ni/Co double hydroxides/Ni/CF positive electrode and a pen ink deposited Ni-coated CF negative electrode. (b2 and b3) SEM images showing Ni/Co double hydroxides with thin nanosheets form a conductive network. Reproduced with permission.[106] Copyright 2017, ACS.

4.3.4. Other transitional metal oxides/metal hydroxides

Several other TMOs/TMHs have also been explored in 1D FSCs, including V_2O_5 and Fe_3O_4. V_2O_5 was studied due to its layered structure to facilitate electrolyte ion transport, variable oxidation states (from V^{2+} to V^{5+}), low cost, and ease of synthesis.[107] Huang *et al.* synthesized ultrathin V_2O_5 nanosheets with a thickness of ~ 2.5 nm, a lateral dimension less

than 10 nm.[108] The ultrathin V_2O_5 nanosheets were sandwiched between interconnected and well-aligned MWCNT scaffolds and then twisted into MWCNT/V_2O_5/MWCNT fibers (see Fig. 11a). The MWCNT scaffolds provided good mechanical robustness and multiple channels for fast electron transport. Subsequently, a symmetric FSC was fabricated using MWCNT/V_2O_5/MWCNT fibers, which delivered a volumetric capacitance of 31 F cm^{-3}, an energy density of 2.1 mW h cm^{-3} at the power density of 1.5 W cm^{-3}.

Fe_3O_4 also offer a wide voltage window at negative potentials, rich abundance, low cost, and environmental friendliness.[109] However, similar to other TMOs/TMHs, their electrical conductivity is low. Thus, carbon materials or conductive polymers have been used to improve their capacitive energy storage performance. Hu *et al.* synthesized a carbon/Fe_3O_4/stainless steel fiber electrode (Fig. 11b).[110] An asymmetric FSC was fabricated by pairing the carbon/Fe_3O_4/stainless steel fiber electrode with a PEDOT/MnO_2/stainless steel fiber electrode, exhibiting an extended voltage window of 2V, a high areal specific capacitance of 60 mF cm^{-2}, and a large energy density of 0.0335 mW h cm^{-2}.

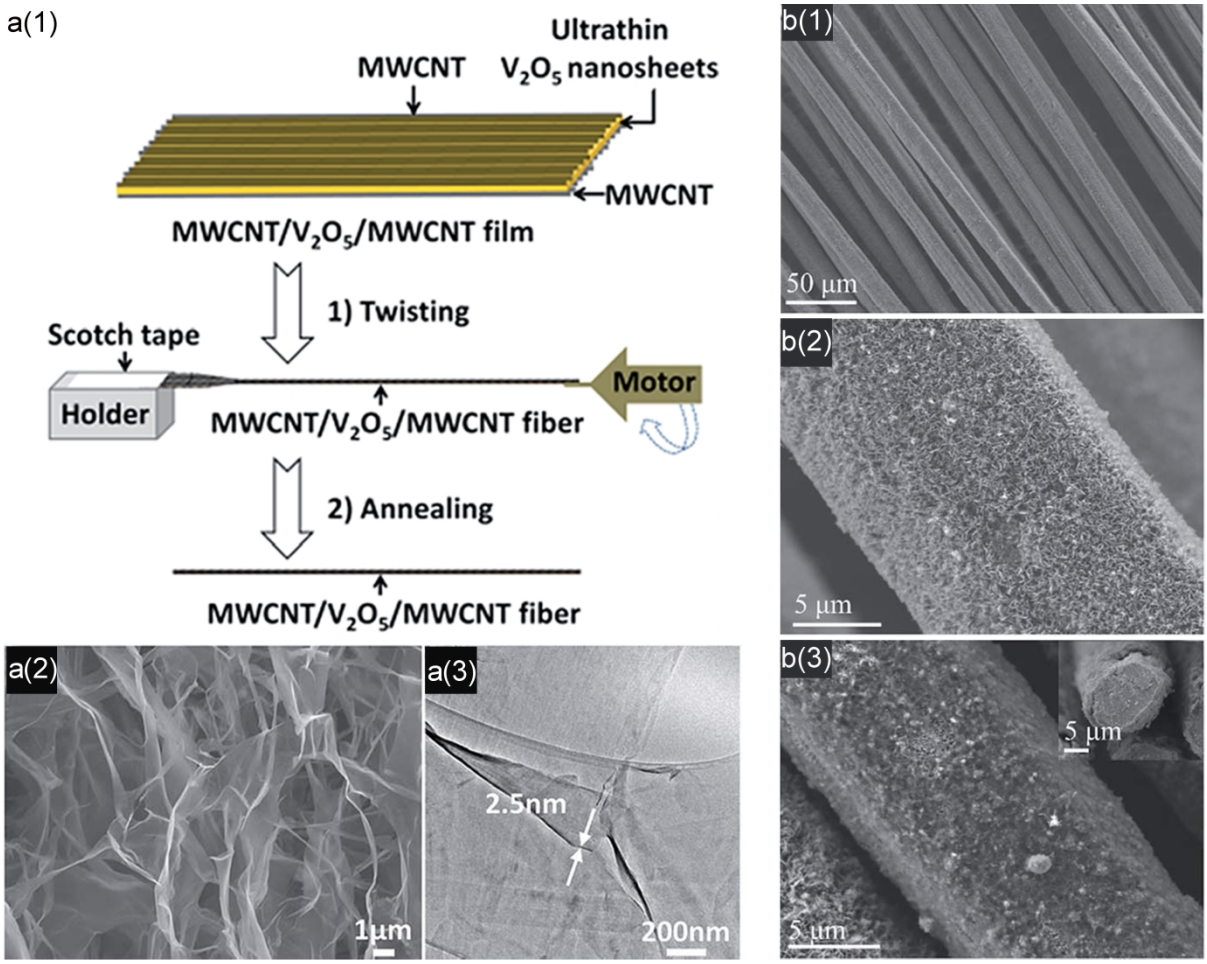

Fig. 11. (a1) Schematic illustration of the synthesis of an MWCNT/V_2O_5/MWCNT fiber. (a2) SEM and (a3) TEM images of V_2O_5 nanosheets. Reproduced with permission.[108] Copyright 2017, RSC. SEM images of Fe3O4 nanoflakes (b2) on a stainless-steel fiber (b1) and subsequently coating a layer of carbon (b3). Reproduced with permission.[110] Copyright 2016, RSC.

4.4. MXenes

In the last few years, MXenes, as a new family of 2D materials, have attracted great interests as capacitive materials for 1D FSCs. MXenes have a general formula of $M_{n+1}X_nT_x$ (n=1–3), where M is an early transition metal (*e.g.,* Ti, Zr, and Mo), X is C or N, and T represents surface terminated groups of –OH, –F or –O.[111] MXenes have several unique

advantages: high electrical conductivity up to 9880 S cm^{-1}, tunable surface hydrophilicity, cation intercalation capability, and a specific capacitance up to 1500 F cm^{-3}.[111, 112] Kim et al. bush-coated Ti carbides on stainless steel wires and assembled an FSC,[113] which exhibited a specific capacitance of 3.09 mF cm^{-1} and an energy density of 210 nW h cm^{-1}. Nearly rectangular shape CV curves were obtained up to 250 mV s^{-1} (Fig. 12b) due to the high electrical conductivity of fiber electrodes. Other than stainless steel wires, MXenes were also coated on other fiber substrates, such as silver-plated Nylon fibers and CFs.[114, 115] However, as we discussed earlier, coating active materials on existing conductive fibers often has a low mass loading and low material utilization rate. It would be more desirable to incorporate MXenes into composite fibers. For example, Razal *et al.* used GO as a host to wet-spun a $Ti_3C_2T_x$ MXnene/GO dispersion into MXene/GO fibers with a high MXene mass loading of ~88 wt.% (Fig. 12c).[116] MXene sheets were orderly aligned between GO liquid crystalline templates. The wet-spun fibers showed a specific capacitance of ~ 341 F cm^{-3} at 0.5 A cm^{-3}. An FSC based on the fibers delivered an energy density of ~ 5.1 mW h cm^{-3} and a power density of 1700 mW cm^{-3}. Alternatively, Rizal *et al.* fabricated flexible yarn electrodes by biscrolling $Ti_3C_2T_x$ MXene with CNT sheets into "BMX yarns" (see Fig. 12d), achieving the highest MXene mass loading of ~ 98 wt.% and displaying specific volumetric, aerial, gravimetric, and linear capacitance of 1083 F cm^{-3}, 3188 mF cm^{-2}, 428 F g^{-1}, and 118 mF cm^{-1}, respectively.[117] An asymmetric FSC was assembled by the BMX yarn with pairing with a biscrolled RuO_2 yarn, delivering an energy density of 61.6 mW h cm^{-3} (168 μW h cm^{-2} and 8.4 μW h cm^{-1}) and a power density of 5428 mW cm^{-3} (14.8 mW cm^{-2} and 741 μW cm^{-1}).

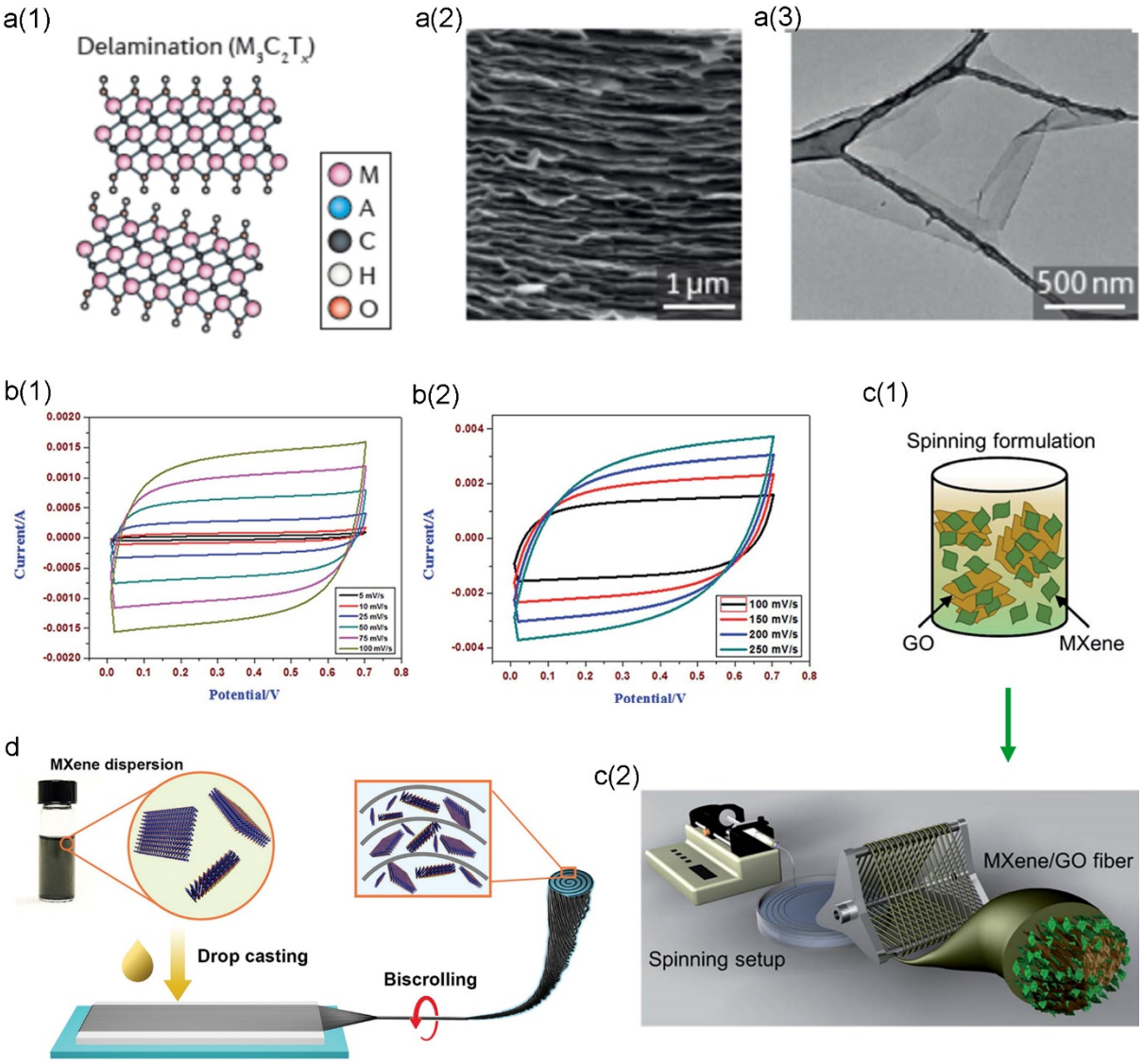

Fig. 12. (a1) Schematic illustration of the atomic structure of $Mo_2TiC_2T_x$, (a2) an SEM image of the cross-sectional of a $Mo_2TiC_2T_x$ film, and (a3) a TEM image of a single-layer $Ti_3C_2T_x$ flake. Reproduced with permission.[111] Copyright 2017, Springer Nature. (b1 and b2) CV curves of an FSC assembled using two Ti carbide-coated stainless steel wires at different scan rates. Reproduced with permission.[113] Copyright 2017, RSC. (c1 and c2) Schematic illustration of the spinning formulation and the fiber spinning of MXene/GO fibers. Reproduced with permission.[116] Copyright 2017, RSC. (d) Schematic illustration of the fabrication process of BMX yarns. Reproduced with permission. [117] Copyright 2017, Wiley-VCH.

Table 2. Summary of recently reported FSCs using 2D materials as electrode materials. (ED: electrochemical deposition; HT: hydrothermal; NA: not available)

		Preparation method	Morphology	Mass loading	Positive electrode	Negative electrode	Electrolyte	Voltage window (V)	Device performance			Note	Ref
									capacitance	Energy density	Power density		
TMDs	MoS_2	Electrochemical intercalation	Nanosheet	6.3 wt%	MWCNTs/MoS_2-GO hybrid fiber	MWCNTs/MoS_2-GO hybrid fiber	PVA/H_2SO_4	0.8	4.8 F cm^{-3} at 0.5 F cm^{-3}	NA	NA	NA	[80]
		Solvothermal	Nanosheet	86 wt%	CNT/MoS_2 hybrid fibers	CNT/MoS_2 hybrid fibers	PVA/H_3PO_4	0.8	135 F cm^{-3} at 5 mV s^{-1}	~ 3 mW h cm^{-3}	0.55 W cm^{-3}	A capacitance retention of 95% after 1000 bending (90°) cycles.	[76]
		HT	Nanosheet	23.03 wt%	rGO/MoS_2 hybrid fibers	rGO/MoS_2 hybrid fibers	PVA/H_3PO_4	0.8	~ 130 F cm^{-3} at 0.1 A cm^{-1}	12.8 mW h cm^{-3}	NA	A tensile strength of 294 MPa at 17.04 wt% MoS_2.	[81]
		HT	Nanosheet	0.0113 mg cm^{-1}	Ti/TiO_2/ MoS_2 coaxial fibers	Ti/TiO_2/ MoS_2 coaxial fibers	PVA/H_3PO_4	0.6	70.6 F cm^{-3} at 5 mV s^{-1}	4.98 mW h cm^{-3}	977.4 mW cm^{-3}	A capacitance retention of 109% when stretched to 333%.	[73]
		Ball-milling (1T phase)	Nanosheet	0.33 mg cm^{-1}	MoS_2/stainless steel wire	MoS_2/stainless steel wire	PVA/LiCl	0.7	119 μF cm^{-1} at 2.5 μA	8.1 nW h cm^{-1}	145 mW cm^{-1}	NA	[84]
TMOs/ TMHs	MnO_2	Reaction with $KMnO_4$	Bulky	NA	MnO_2/CFs	MnO_2/CFs	PVA/H_3PO_4	0.8	2.5 F cm^{-3} at 0.02 A cm^{-3}	0.22 mW h cm^{-3}	0.4 mW cm^{-3}	A capacitance retention of ~ 100% under various bending angles (0–90°)	[89]
		ED	Nanosheets	NA	MnO_2/CFs	MnO_2/CFs	PVA/Na_2SO_4	1.0	NA	3.8 mW h cm^{-3}	89 mW cm^{-3}	A capacitance retention of ~ 100% after 2000 bending cycles at 90°.	[91]

HT	Nanosheets	0.12 mg cm^{-2}	MnO_2/CFs	rGO/CFs	PVA/LiCl	1.5	87.1 F kg^{-1} at 1.25 A g^{-1}	27.2 Wh kg^{-1}	979.7 W kg^{-1}	Woven into cotton textiles.	[92]
ED	Nanoflakes	NA	MnO_2/rGO/ CF	rGO/CFs	PAAK/KCl	1.6	NA	1.23 mW h cm^{-3}	270 mW cm^{-3}	A capacitance retention of 96.8% after 500 bending cycles at 180°.	[94]
ED	Nanoflakes	NA	MnO_2/rGO/ CF	rGO/ copper wire	PAAK/KCl	1.6	2.54 F cm^{-3} at 0.2 mA cm^{-2}	0.9 mW h cm^{-3}	8 mW cm^{-3}	A capacitance retention of 96.3% after 500 bending cycles at 90°.	[93]
Reaction with $KMnO_4$	Nanosheets	NA	MnO_2/Holey rGO fiber	MnO_2/Holey rGO fiber	PVA/H_3PO_4	0.8	16.7 mF cm^{-2} at 0.05 mF cm^{-2}	NA	NA	No obvious capacitance changes under bending.	[62]
ED	Nanoflakes	NA	PPy/MnO_2/ CFs	PPy/MnO_2/CFs	PVA/H_3PO_4	0.8	69.3 F cm^{-3} at 0.1 A cm^{-3}	6.16 mW h cm^{-3}	40 mW cm^{-3}	No obvious capacitance changes under folding and rolling up.	[98]
ED	Nanosheets	67 wt%	MnO_2/ PEOOT: PSS/ CNT fiber	Ordered microporous carbon/ CNT fiber	CMC/Na_2SO_4	1.8	23.4 F cm^{-3} at 0.085 A cm^{-3}	11.3 mW h cm^{-3}	30 mW cm^{-3}	A capacitance retention of ~ 100% after 5000 bending cycles.	[97]
ED	Nanosheets	NA	PPy/MnO_2/ rGO/stainless steel yarn	PPy/MnO_2/ rGO/stainles teel yarn	PVA/H_3PO_4	0.8	68.52 F cm^{-3}	6 mW h cm^{-3}	0.844 W cm^{-3}	Stable under various shape deformation cycles. Woven into a fabric.	[99]
ED	Flower-like nanostruct	NA	PPy/MnO_2/ SWCNTS-coated cotton yarn	PPy/MnO_2/ SWCNTS-coated	PVA/H_3PO_4	0.8	1.49 F cm^{-2} at 1 mV s^{-1}	0.033 mW h cm^{-2}	0.67 mW cm^{-2}	No obvious capacitance changes under bending.	[35]

		ure With nanoplate			cotton yarn						
$NiCo_2O_4$	ED	Nanoflake	NA	3D-$NiCo_2O_4$/Ni wire	3D-$NiCo_2O_4$/Ni wire	PVA/KOH	1.0	30 F g^{-1} or 3 F cm^{-3} at 5 mV s^{-1}	2.18 W h kg^{-1} or 0.21 mW h cm^{-3}	21.6 W kg^{-1} or 2.1 mW cm^{-3}	No obvious capacitance changes under bending at 90°.	[103]
$Ni(OH)_2$	In situ transformation	Nanosheet	NA	$Ni(OH)_2$/ rGO/Ni wire	rGO/Ni wire	PVA/KOH	1.6	69 F g^{-1} at 2 A g^{-1}.	0.83 mW h cm^{-3}	54 mW cm^{-3}	No obvious capacitance changes under bending.	[104]
NiO/ $Ni(OH)_2$	ED and dealloying method	Nanoflower	NA	NiO/ $Ni(OH)_2$/ Cu-Ni wire	CFs	PVA/KOH	1.45	31.6 mF cm^{-2} or 3.16 F cm^{-3} at 0.4 mA cm^{-2}	0.011 mW h cm^{-2}	7.8 mW cm^{-2}	No obvious capacitance changes after 1400 bending cycles.	[105]
Ni-Co double hydroxide	ED	Nanosheet	NA	Ni-Co double hydroxide/Ni-coated CFs	Pen ink/Ni-coated CFs	PVA/KOH	1.55	28.67 mF·cm^{-2}	9.57 μWh cm^{-2}	1841.1 μW cm−2	NA	[106]
V_2O_5	Chemical reaction	Nanosheet	90 wt%	MWCNT/V_2O_5/MWCNT fibers	MWCNT/V_2O_5/MWCNT fibers	PVA/LiCl	0.8	31 F cm^{-3} at 1 A cm^{-3}	2.1 mW h cm^{-3}	1.5 W cm^{-3}	Mechanically stable under knotting.	[108]
Fe_2O_3	ED	Nanosheet	0.142 mg cm^{-1}	PEDOT/ MnO_2/ stainless steel fiber	Carbon/ Fe_3O_4/ stainless steel fiber	PVA/LiCl	2.0	60 mF cm^{-2} or 7.2 F cm^{-3} at 0.9 mA	0.0335 mW h cm^{-2} or 4.02 mW h cm^{-3}	0.6 mW cm^{-2} or 72 mW cm^{-3}	No obvious capacitance changes under bending, knotting and winding; Woven into a wristband.	[110]

MXenes	titanium carbide	Selective extraction of Al from the precursor Ti_2AlC	Nanosheet	0.33 mg cm^{-1}	titanium carbide/ stainless steel wire	titanium carbide/ stainless steel wire	PVA/KOH	0.7	3.09 mF cm^{-1},	210 nW h cm^{-1}	~ 58.3 μW cm^{-1}	No obvious capacitance changes at bended states	[113]
	$Ti_3C_2T_x$	Selective extraction of Al from the precursor Ti_2AlC	Nanosheet	2 mg cm^{-1}	MXene/ PEDOT-PSS/CF	MXene/ PEDOT-PSS/CF	PVA/H_3PO_4	0.5	~126.3 mF cm^{-1} at 2 mV s^{-1}	NA	NA	A capacitance retention over 95% under bending and twisting.	[115]
		Dropping-mild baking	Nanosheet	0.7 mg cm^{-1}	$Ti_3C_2T_x$/ silver plated nylon fiber	$Ti_3C_2T_x$/ silver plated nylon fiber	PVA/H_2SO_4	0.4	50 mF cm^{-1} or 328 mF cm^{-2} at 2 mV s^{-1}	7.3 μW h cm^{-2}	132 μW cm^{-2}	A capacitance retention over 90% under bending and 80% under twisting; Slightly capacitance decrease after 1000 bending cycles at 100°.	[114]
		Minimally intensive layer delamination	Nanosheet	97.4 wt%	RuO_2/CNT yarn	$Ti_3C_2T_x$/ CNT yarn	PVA/H_2SO_4	1.5	203 F cm^{-3} or 554 mF cm^{-2}, 123 F g^{-1}, and 27.8 mF cm^{-1} at 2 mA cm^{-2}	61.6 mW h cm^{-3} or 168 μWh cm^{-2} or 8.4 μW h cm^{-1}	5428 mW cm^{-3} or 14.8 mW cm^{-2} or 741 μW cm^{-1}	A capacitance retention of ~ 100% after 1000 bending cycles at 90°; And woven into a cotton fabric.	[117]
		Selective extraction of Al from the precursor Ti_2AlC	Nanosheet	~ 88 wt%	$Ti_3C_2T_x$/ rGO composite fiber	$Ti_3C_2T_x$/ rGO composite fiber	PVA/H_2SO_4	0.8	NA	~ 5.1 mW h cm^{-3}	1700 mW cm^{-3}	NA	[116]

5. 2D materials for 1D cable-shaped batteries

5.1. 2D materials for 1D cable-shaped lithium-ion batteries

The commercialization of LIBs by Sony in 1991 revolutionizes portable electronics, and LIBs have become the most widely used energy storage solution for portable electronics. LIBs typically consist of an anode, a cathode, electrolyte, and a separator that allows the passing of Li^+ but block electron transfers between the anode and cathode. LIBs store energy via the reversible intercalation/de-intercalation of Li^+ between the anode and cathode. Some requirements for electrode materials used in LIBs include high reversible capacity for Li^+ intercalation, good structural stability, fast Li^+ diffusion rate, long cycle life, good safety, low cost, and environmental friendliness.[20, 118] 2D materials including graphene, TMDs, TMOs, and TMHs. have attracted many interests as electrode materials for LIBs because of their unique layered structures which may enable fast Li^+ diffusion rate.[19, 119, 120] 1D cable-shaped LIBs (CLIBs) is regarded as a new type of flexible LIBs, which may be used to fulfill the new flexibility or wearability requirements of emerging portable electronics. To date, 2D materials have mainly been explored as anode materials in CLIBs because of their low Li intercalation voltages versus Li/Li^+.[121] In the following two sub-sessions, the studies of various 2D materials as anode materials in CLIBs are summarized.

5.1.1. Graphene

Graphite is the dominate anode materials in LIBs since 1990s because it is abundant, chemically stable, cheap and environmentally friendly. It has a theoretical capacity of ~ 372 mAh g^{-1} (forming LiC_6 stoichiometry) and possesses high Columbic efficiency, low and flat potential. Thus, graphite dominates the anode material market of commercial LIBs.[118, 122]

Nevertheless, the capacity limit of graphite limits the energy density of LIBs. Besides, the Li^+ diffusion rate in graphite is low, hindering high-power applications of LIBs.[118, 122] In contrast, stacked graphene with expanded interlayer spacings may facilitate the intercalation/de-intercalation of Li^+.[19, 123] Besides, the diffusion rate of Li^+ on graphene is fast (~ 10^{-7}–10^{-6} cm^2 s^{-1}), which may enable high power applications.[124] Further, a theoretical study predicted that graphene sheets (ca. 0.7 nm thick) could deliver higher energy storage capacity (by forming Li_4C_6 stoichiometry).[125] However, the utilization of graphene as anode materials in LIBs suffers from the low Columbic efficiency and large irreversible capacity due to the formation of solid electrolyte interface (SEI) and the undesirable reactions between Li^+ with oxygen-containing groups on graphene.[118] For example, Lian *et al.* synthesized few-layer (~4 layers) graphene sheets and applied them as anode materials of LIBs. A reversible capacity ~1200 mA h g^{-1} was achieved at the first charging/discharging cycle, but only 848 mA h g^{-1} can be retained after 40 cycles.[126]. Some research efforts were devoted to graphene-based composite electrodes containing other anode materials.[127] Graphene serves as a conductive addictive or frameworks to bridge adjacent anode materials to ensure a fast electron transfer. It may also suppress the volume expansion/extraction and aggregation of some anode materials during cycling. To the best of our knowledge, few studies have explored graphene in CLIBs

5.1.2. Titanium oxide-based materials

TiO_2 has the advantage of high safety and excellent cycling life. Besides, TiO_2 has a high energy storage capacity up to 330 mAh g^{-1} together with structural diversity.[118, 122] Geng *et al.* synthesized TiO_2 sheets via a exfoliation strategy. Then a TiO_2/rGO fiber electrode was fabricated by wet-spinning of 2D TiO_2 sheets with GO nanosheets (see Fig. 13a).[128] The

composite fiber electrode exhibited an energy storage capacity of 0.028 mAh cm^{-1} at 0.0085 mA.

5.1.3. MoS_2

2D MoS_2 has also been explored as anode materials in 1D CLIBs. The layered structure of MoS_2 enables the efficient intercalation and de-intercalation of Li^+ ions, and MoS_2 has an energy storage capacity of 670 mAh g^{-1}.[129] Peng *et al*. synthesized MoS_2 nanosheets on CNT sheets and subsequently twisted the MoS_2 coated CNT sheets into fibers (Fig. 13b).[130] CNTs serve as a conductive scaffold to enhance the electron transfer and buffer the volume changes of MoS_2 during charging/discharging cycles. A CLIB was fabricated by pairing the CNT/MoS_2 composite fiber with a Li wire, followed by sealing the two electrodes in a heat-shrinkable tube with 1 M LiPF6 as the electrolyte and a separator. This CLIB exhibited an energy storage capacity of 1250 mAh g^{-1} at 0.2 A g^{-1}.

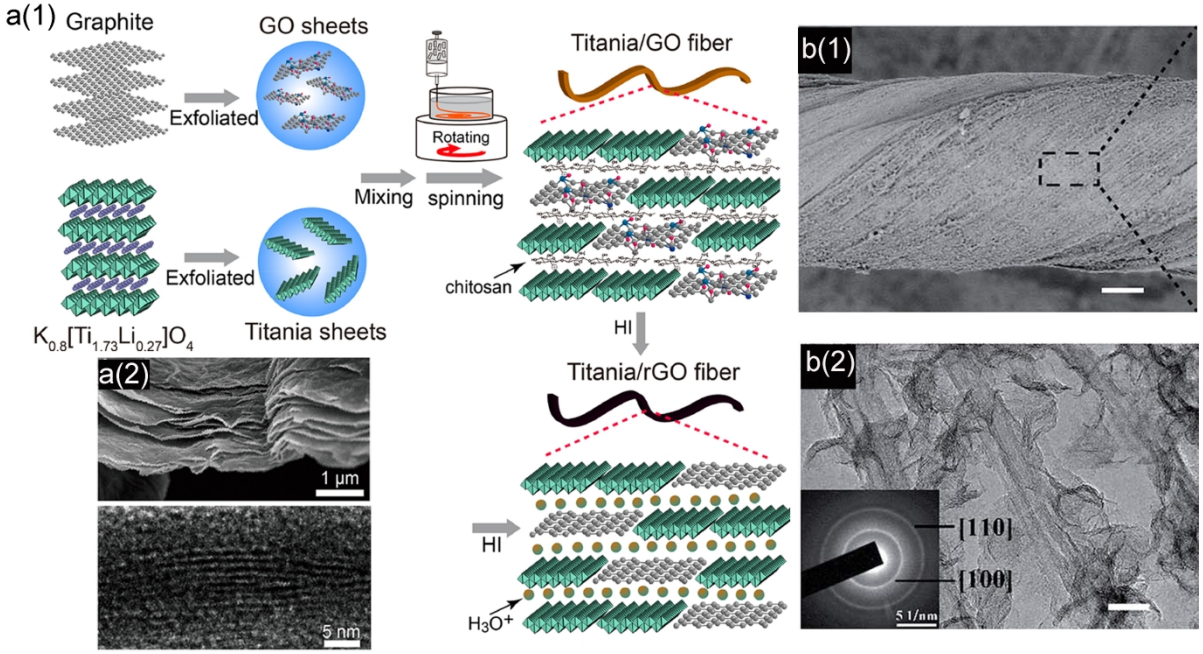

Fig. 13. (a1) Schematic illustration of the fabrication of a TiO_2/rGO composite fiber. (a2) SEM (upper panel) and TEM (lower panel) images for the HI-reduced TiO_2/rGO fiber. Reproduced with permission.[128] Copyright 2017, ACS. (b1) SEM images of the aligned CNT/MoS_2 hybrid fiber and (b2) TEM images of MoS_2 nanosheets with an inserted electron diffraction pattern. Reproduced with permission.[130] Copyright 2015, RSC.

5.2. 2D materials for other 1D cable-shaped batteries

Besides LIBs, several other types of batteries, such as Na-ion, Ni-Zn, and Ni-Fe batteries, have been extensively studied. They are expected to complement or replace LIBs in some applications due to their different characteristics. 2D materials have also been used to assemble 1D CBs based on some of these battery types.

5.2.1. 2D materials for 1D cable-shaped sodium-ion batteries

Because of the abundant availability and low cost of Na, NIBs have been studied to complement LIBs.[131, 132] As illustrated in Fig. 14a, Yang *et al.* first synthesized WS_2 nanosheets on a porous 3D carbon form derived from a polymer foam. Then, N-doped graphene quantum dots were deposited on WS_2 nanosheets, resulting in the NGQDs-WS_2/3DCF composite.[133] The 2D layered WS_2 can be used as an anode material for NIBs because of its large theoretical capacity of 432 mA h g^{-1}, large interlayer spacing of 0.62 nm, and weak van der Waals interactions among individual layers, which enable easy intercalation/de-intercalation of Na^+ with small volume change. The NGQDs-WS_2/3DCF composite exhibited an energy storage capacity of 268.4 mA h g^{-1} at 2000 mA g^{-1}, and a long life with 97.1% capacity retention after 1000 charging/discharging cycles. A 1D Na-ion cable

battery was demonstrated using the NGQDs-WS_2/3DCF anode together with a $Na_{0.44}MnO_4$ cathode, a winding copper wire current collector, 1 M $NaPF_6$ electrolyte, a separator and a shrinkable plastic tube as the insulating tube (Fig. 14a). The 7 cm long cable-shaped Na-ion battery delivered an energy storage capacity of ~ 1.3 mA h at the current of 3 mA.

5.2.2. 2D materials for 1D cable-shaped zinc-based batteries

Zn possesses several advantages as a battery material, low cost, low toxicity, and good chemical stability in air. Therefore, various Zn-based batteries have been created. For example, Lu *et al.* demonstrated a 1D Ni–Zn battery based on a Ni–NiO heterostructural nanosheet-coated CF cathode, a Zn wire anode, and PVA/KOH gel electrolyte (Fig. 14b).[134] The Ni-Zn battery exhibited an energy storage capacity of 116.1 μA h cm^{-3} at 3.7 A g^{-1}. Xiao *et al.* assembled a 1D Ni-Fe battery using an Mn-NiO nanosheet/CuO/Cu fiber anode, an Mn-Fe_2O_3 nanoplates/CuO/Cu fiber cathode and PVA/KOH gel electrolyte (Fig. 14c).[135] The Ni-Fe battery delivered an energy storage capacity of 46 mA h g^{-1} at the current density of 2.5 A cm^{-3} and 91.2% capacity retention after 30000 charging/discharging cycles. The good performance was attributed to the Mn doping in NiO nanosheets and Fe_2O_3 nanoplates, which optimizes the electronic structures of the anode and cathode materials.

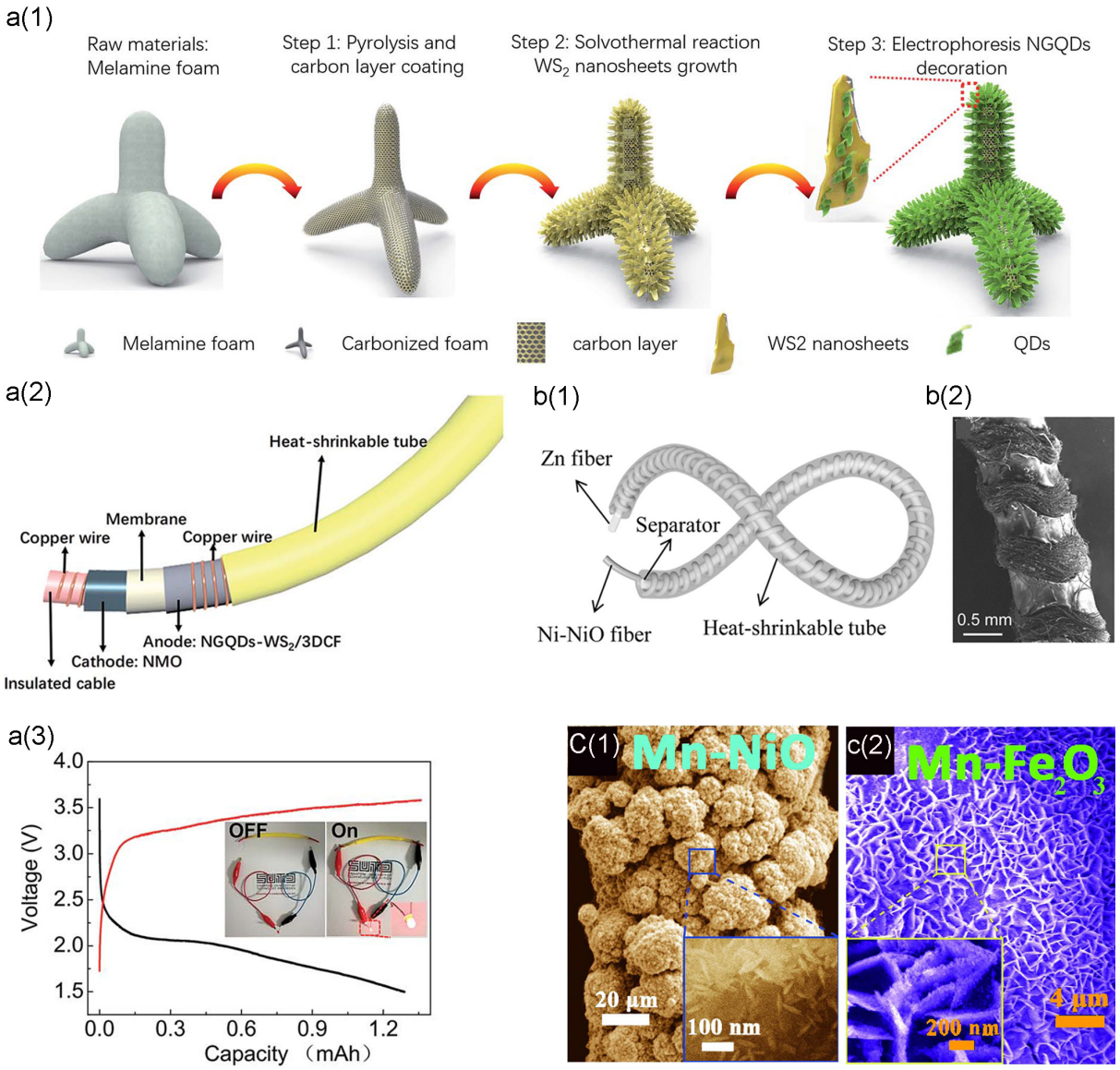

Fig. 14. (a1) Schematic illustration of the synthesis of an NGQDs-WS_2/3DCF composite. (a2) Schematic illustration of the structure of a 1D Na-ion battery. (a3) Charging/discharging curves of the battery at the current of 3 mA (the third cycle after two pre-activation cycles). Reproduced with permission.[133] Copyright 2018, RSC. (b1) Schematic illustration of the structure of a 1D Ni-NiO//Zn battery. (b2) An SEM image of the Ni-NiO//Zn battery. Reproduced with permission.[134] Copyright 2017, Wiley-VCH. (c) SEM images of Mn-doped NiO nanosheets and Mn-doped Fe_2O_3 nanoplates. The inserts show the enlarged view of selected regions. Reproduced with permission.[135] Copyright 2018, Elsevier.

Table 3. Summary of 2D materials applied in 1D cable-shaped batteries.

Type	Structure	Anode	Cathode	Separator	Electrolyte	Sealing	Capacity	Note	Ref.
Li-ion	twisted	Li wire	MoS_2/CNT fiber	No	1 M $LiPF_6$	Heat-shrinkable tube	1250 mA h g^{-1} at 0.2 A g^{-1} (based on the mass of cathode)	NA	[130]
Li-ion	parallel	TiO_2/rGO fiber	Li wire	Celgard separator	1 M $LiPF_6$	Heat-shrinkable tube	0.028 mA h cm^{-1} at 0.0085 mA	Stable voltage under bending.	[128]
Na-ion	coaxial	NGQDs-WS_2/3DCF	$Na_{0.44}MnO_2$	Glass fiber filter	1 M $NaPF_6$	Heat-shrinkable tube	0.156 mA h cm^{-1} at 3 mA	Stable lighting a LED under bending. Used as a wrist strap.	[133]
Ni-Zn	coaxial	Zn wire	Ni-NiO nanosheets/carbon cloth fiber	No	PVA/KOH	Heat-shrinkable tube	116.1 μA h cm^{-3} at 3.7A g^{-1}	No obvious performance changes under bending.	[134]
Ni-Fe	coaxial	Mn-NiO nanosheets/ CuO/Cu fiber	Mn-Fe_2O_3 nanoplates/ CuO/Cu fiber	No	PVA/KOH	Heat-shrinkable tube	46 mA h cm^{-3} at 2.5 A cm^{-3}	No obvious capacity changes under bending at 0–180°.	[135]

6. Summary and outlooks

2D materials exhibit unique advantages as electrode materials for SCs and batteries. They include: (1) large surface areas with abundant activate cites to enable physical adsorption of electrolyte ions or surface redox reactions, (2) flat 2D surfaces to allow fast ion diffusion, (3) layered structures to host ion intercalation/de-intercalation, (4) good mechanical strength and flexibility, and (5) high electrical conductivity from some 2D materials, such as 1T phase TMDs and MXenes.

We have summarized recent research advances in exploring various 2D materials for fabricating 1D fiber or cable-shaped electrochemical energy storage devices. The current research strategies to improve 2D materials' performance in energy storage have been focused on the following four aspects. (1) Engineering physical properties of 2D materials. For example, controlling the lateral dimension of 2D nanosheets can tailor their electronic and ionic conductivity. Creating nanosized holes in nanosheets can increase their surface area and create efficient mass transfer channels. (2) Modulating chemical properties of 2D materials. For example, partially replacing Co in Co_3O_4 or $LiCoO_2$ with cheaper and more environmentally friendly elements can concurrently improve electrical conductivity, stability and provide additional active sites for redox reactions. Mo_2S with 1T phase can be selectively synthesized, which is 10^7 times more conductive than its 2H phase counterpart. (3) Constructing nanocomposites to create synergistic effects. For example, graphene sheets are often used as substrates for 2D TMOs/TMHs, TMDs or Si NWs, which serve as mechanical supports or cages to suppress volume expansion, electron transfer highways, and spacers to avoid nanomaterial aggregation. (4) Designing fiber (cable) electrodes with optimal hierarchical architectures. For example, in a core-sheath fiber electrode based on PPy/MnO_2/stainless steel wires, coating graphene nanosheets on the stainless-steel wires

increase active sites for anchoring MnO_2 nanoparticles, and the PPy coating increases the electrical conductivity and prevents the detachment of MnO_2 nanoparticles.

Although significant research efforts have been devoted to creating high-performance 1D electrochemical energy storage devices using 2D materials, many challenges remain. In our view, the following research topics are critical to realize their practical applications.

Controlling the re-tacking of 2D materials. A key challenge in using 2D materials as 1D fiber electrode materials is to prevent the uncontrollable re-stacking of nanosheets during the fiber electrode fabrication. For example, when graphene nanosheets are assembled into 1D fibers, it is common to obtain a specific surface area around 20 $m^2 g^{-1}$, which is much smaller than that of pristine graphene. The uncontrollable re-stacking of 2D materials would significantly reduce their electrolyte ion accessible surface areas and increase the mass transfer resistance of ions. Thus, it remains a challenge in producing fiber electrodes containing densely packed 2D materials while maintaining their good rate performance. Future research may be carried out by either changing intrinsic properties of 2D materials or rationally designing and controlling nanoscale and macroscale structures of fiber electrodes.

Increasing the electrical conductivity of fiber electrodes. The electrical conductivity of electrodes strongly influences the rate performance of both SCs and batteries. Especially, electrons must travel a long distance along 1D electrodes, increasing the electrical conductivity of fiber electrode is critical for obtaining high-performance 1D electrochemical energy storage devices. Although graphene, metallic TMDs (1T phase MoS_2), and MXenes have high electrical conductivity, their practical applications in 1D electrodes still face many issues. For example, the commonly used GO nanosheets have poor electrical conductivity. Various reduction methods used to convert GO to graphene fail to restore the intrinsic electrical conductivity of graphene. Scalable methods to synthesize well-dispersed conductive graphene nanosheets are still missing. Although 1T MoS_2 is highly conductive, it is

thermodynamically not stable and can easily convert to a more stable but less conductivity 2H phase. Further research needs to find solutions to incorporate highly conductive 2D materials into 1D fiber electrodes properly and retain their properties under long term charging/discharging conditions.

Aligning 2D materials in 1D fibers. Many approaches can be used to include 2D materials in 1D fibers as introduced in this review. 2D materials in the forms of nanosheets, nanowires, and nanoparticles can be deposited on the outer surface of 1D fiber substrates. Alternatively, they may be incorporated inside porous 1D fibers. However, few studies have so far been able to control the alignment of 2D materials in 1D fibers precisely. Many unique characteristics of 2D materials are anisotropic. For example, the mass transfer of electrolyte ions depends on the alignment of 2D nanosheets, and the lateral channels of 2D materials would be preferred. The alignment of 2D nanosheets would also affect the contract resistance among individual nanosheets. Thus, it is necessary to control the alignment 2D nanosheets in order to yield the optimal energy storage performance.

Improving performance stability. When 1D electrochemical energy storage devices are integrated into portable/wearable electronics, they expected to perform well over the entire lifespan of these electronics. However, the poor chemical/electrochemical/cycling stability of some 2D materials is a limiting factor to achieve this. For example, MXenes can be oxidized easily under anodic potentials in aqueous electrolytes. Further, in intercalation-based SCs and batteries, 2D materials may have a large volume expansion due to incompatibility between intercalation ions and their interlayer spacing, resulting in poor structural stability. In addition to improving intrinsic stability of these 2D materials, developing novel electrolytes to create suitable electrolyte-electrode interfaces or hybridizing with other materials should also be explored to improve the stability of 2D materials.

Deepening fundamental chemistry understandings. Many studies have reported excellent performance of various 2D materials in 1D electrochemical energy storage devices. However, the good understandings of their energy storage mechanisms are often missing. For example, the surface chemistry of MXenes under different energy storage conditions has not been fully explored. The detailed contributions of different doping elements, such as B, P, and S or their combinations, in the energy storage behaviors of graphene-family materials, remain elusive. In general, the structure-property relationship of many new 2D materials has not been studied in detail. Therefore, more experimental and computational studies would be required to improve fundamental chemistry understandings, which would guide us to achieve better engineering designs in 2D material based 1D electrochemical energy storage devices.

Increasing energy storage capacity. The total energy storage capacity of FSCs and CBs directly correlates with their total volume, which is determined by their length and diameter. Many recent studies only reported FSCs and CBs in short length or small diameters because such small devices often yield better performance characteristics due to the short electron and ion transport distance. Although small devices are useful for some applications, more applications would require large volume energy storage devices to provide higher energy storage capacity. This could be achieved by increasing either the length or diameter of FSCs and CBs. However, with the increase of device length or diameter, their electrochemical performance often deteriorates due to increased electrical and diffusion resistances along axis or radial directions.[69, 72] The excellent electrochemical performance demonstrated in short length and small diameter devices often cannot be directly translated to long and large diameter devices. Researchers are generally addressing this challenge by two approaches. One is to use more conductive substrates (*e.g.,* stainless steel yarns) or electrode materials (*e.g.,* TiN, VN).[99, 136, 137] The other is to integrate multiple short FSCs and CBs in series

and parallel.[138] Both approaches have their limitations to elevate the total energy storage capacity, which requires extensive future research efforts.

Standardizing performance reporting metrics. Following the discussion above, the performance of 1D FSCs and CBs depends on their length and diameter. 1D FSCs and CBs devices with smaller diameters and shorter length often show better gravimetric or volumetric specific energy and power densities and rate capability due to their shorter electron and ion transport distance.[69, 72] This phenomenon is similar to the performance dependence on the thickness of electrode materials in 2D electrochemical energy storage devices. Commercial electrodes usually contain 100 to 200 μm thick or about 10 mg/cm^2 of active electrode materials. A thin electrode may yield better energy storage performance results due to reduced transport distance.[139] It is prevalent in this area that many important metrics are omitted in the reported data. In addition to the metrics proposed by Gogotsi et al. for textile energy storage devices,[13] it is essential to include both length and diameter of tested devices and their electrodes. Future studies should also carefully investigate how the performance of 1D FSCs and CBs depends on their length and diameter and optimize these two critical parameters for practical applications.

Achieving scalable device manufacture. Scalable manufacture of 1D FSCs and CBs is critical for realizing their commercialization. To date, most of FSCs and CBs are fabricated by manually in research labs, and the scalability of their fabrication method is rarely studied. Scalable fabrication of delicately designed 1D electrodes in a cost-effective manner is complicated, which typically involves coating of active materials on 1D fibers, pairing of 1D electrodes in different configurations (*e.g.,* coaxial, twisted and parallel), and encapsulation of completed 1D devices. One study tried to address this challenge by integrating all materials and fabrication steps in a continuous process.[140] The reported synchronized deposition method can continuously fabricate FSCs from aligned CNT composite arrays with

other electrode materials in minutes. Along with this direction, we expect that significant research efforts would be required to optimize different fabrication methods so various new 1D FSCs and CBs can be scalably produced to meet market demands.

Acknowledgment

The authors acknowledge financial support from Australian Research Council under the Future Fellowships scheme (FT160100107) and Discovery Project (DP180102210)

References

[1] W. Zeng, L. Shu, Q. Li, S. Chen, F. Wang, X.M. Tao, Adv. Mater., 26 (2014) 5310-5336.

[2] M. Stoppa, A. Chiolerio, Sensors, 14 (2014) 11957-11992.

[3] A.J. Bandodkar, J. Wang, Trends in Biotechnology, 32 (2014) 363-371.

[4] A.J. Bandodkar, I. Jeerapan, J. Wang, ACS Sensors, 1 (2016) 464-482.

[5] X.M. Tao, Wearable Electronics and Photonics, Woodhead Publishing2005.

[6] T. Someya, Stretchable Electronics, Wiley-VCH Verlag GmbH & Co. KGaA2012.

[7] J.A. Rogers, T. Someya, Y.G. Huang, Science, 327 (2010) 1603-1607.

[8] M.L. Hammock, A. Chortos, B.C.K. Tee, J.B.H. Tok, Z.A. Bao, Adv. Mater., 25 (2013) 5997-6037.

[9] S. Bauer, S. Bauer-Gogonea, I. Graz, M. Kaltenbrunner, C. Keplinger, R. Schwodiauer, Adv. Mater., 26 (2014) 149-162.

[10] D. Yu, Q. Qian, L. Wei, W. Jiang, K. Goh, J. Wei, J. Zhang, Y. Chen, Chem. Soc. Rev., 44 (2015) 647-662.

[11] S. Zhai, H.E. Karahan, L. Wei, Q. Qian, A.T. Harris, A.I. Minett, S. Ramakrishna, A.K. Ng, Y. Chen, Energy Storage Mater., 3 (2016) 123-139.

[12] L. Hu, M. Pasta, F. La Mantia, L. Cui, S. Jeong, H.D. Deshazer, J.W. Choi, S.M. Han, Y. Cui, Nano Lett., 10 (2010) 708-714.

[13] K. Jost, G. Dion, Y. Gogotsi, J. Mater. Chem. A, 2 (2014) 10776-10787.

[14] Y. Zhang, Y. Zhao, J. Ren, W. Weng, H. Peng, Adv. Mater., 28 (2016) 4524-4531.

[15] M. Li, M. Zu, J. Yu, H. Cheng, Q. Li, Small, 13 (2017) 1602994.

[16] S. Seyedin, M.S. Romano, A.I. Minett, J.M. Razal, Sci. Rep., 5 (2015) 14946.

[17] G. Wang, L. Zhang, J. Zhang, Chem. Soc. Rev., 41 (2012) 797-828.

[18] L.L. Zhang, X. Zhao, Chem. Soc. Rev., 38 (2009) 2520-2531.

[19] L. Shi, T. Zhao, J. Mater. Chem. A, 5 (2017) 3735-3758.

[20] N. Nitta, F. Wu, J.T. Lee, G. Yushin, Mater. Today, 18 (2015) 252-264.

[21] K.S. Novoselov, A.K. Geim, S.V. Morozov, D. Jiang, Y. Zhang, S.V. Dubonos, I.V. Grigorieva, A.A. Firsov, Science, 306 (2004) 666-669.

[22] M.J. Allen, V.C. Tung, R.B. Kaner, Chem. Rev., 110 (2009) 132-145.

[23] V. Chabot, D. Higgins, A. Yu, X. Xiao, Z. Chen, J. Zhang, Energy Environ. Sci., 7 (2014) 1564-1596.

[24] Y. Zhu, S. Murali, W. Cai, X. Li, J.W. Suk, J.R. Potts, R.S. Ruoff, Adv. Mater., 22 (2010) 3906-3924.

[25] D. Akinwande, N. Petrone, J. Hone, Nat. Commun., 5 (2014) 5678.

[26] A.J. Mannix, B. Kiraly, M.C. Hersam, N.P. Guisinger, Nat. Rev. Chem., 1 (2017) 0014.

[27] K. Novoselov, A. Mishchenko, A. Carvalho, A.C. Neto, Science, 353 (2016) aac9439.

[28] B. Mendoza-Sánchez, Y. Gogotsi, Adv. Mater., 28 (2016) 6104-6135.

[29] F. Bonaccorso, L. Colombo, G. Yu, M. Stoller, V. Tozzini, A.C. Ferrari, R.S. Ruoff, V. Pellegrini, Science, 347 (2015) 1246501.

[30] K.S. Kumar, N. Choudhary, Y. Jung, J. Thomas, ACS Energy Lett., 3 (2018) 482-495.

[31] L. Peng, Y. Zhu, D. Chen, R.S. Ruoff, G. Yu, Adv. Energy Mater., 6 (2016) 1600025.

[32] X. Yu, S. Yun, J.S. Yeon, P. Bhattacharya, L. Wang, S.W. Lee, X. Hu, H.S. Park, Adv. Energy Mater., 8 (2018) 1702930.

[33] Z. Lei, J. Zhan, L. Tang, Y. Zhang, Y. Wang, Adv. Energy Mater., 8 (2018) 1703482.

[34] M. Chhowalla, H.S. Shin, G. Eda, L.-J. Li, K.P. Loh, H. Zhang, Nat. Chem., 5 (2013) 263.

[35] N. Liu, W. Ma, J. Tao, X. Zhang, J. Su, L. Li, C. Yang, Y. Gao, D. Golberg, Y. Bando, Adv. Mater., 25 (2013) 4925-4931.

[36] L. Liu, Y. Yu, C. Yan, K. Li, Z. Zheng, Nat. Commun., 6 (2015) 7260.

[37] C. Choi, S.H. Kim, H.J. Sim, J.A. Lee, A.Y. Choi, Y.T. Kim, X. Lepró, G.M. Spinks, R.H. Baughman, S.J. Kim, Sci. Rep., 5 (2015) 9387.

[38] Z. Liu, F. Mo, H. Li, M. Zhu, Z. Wang, G. Liang, C. Zhi, Small Methods, 2 (2018) 1800124.

[39] H. Lee, M. Kim, I. Kim, H. Lee, Adv. Mater., 28 (2016) 4541-4548.

[40] X. Lu, M. Yu, G. Wang, Y. Tong, Y. Li, Energy Environ. Sci., 7 (2014) 2160-2181.

[41] S. Senthilkumar, Y. Wang, H. Huang, J. Mater. Chem. A, 3 (2015) 20863-20879.

[42] C. Zhong, Y. Deng, W. Hu, J. Qiao, L. Zhang, J. Zhang, Chem. Soc. Rev., 44 (2015) 7484-7539.

[43] X. Huang, X. Qi, F. Boey, H. Zhang, Chem. Soc. Rev., 41 (2012) 666-686.

[44] M.D. Stoller, S. Park, Y. Zhu, J. An, R.S. Ruoff, Nano Lett., 8 (2008) 3498-3502.

[45] W.S. Hummers Jr, R.E. Offeman, J. Am. Chem. Soc., 80 (1958) 1339-1339.

[46] D.C. Marcano, D.V. Kosynkin, J.M. Berlin, A. Sinitskii, Z. Sun, A. Slesarev, L.B. Alemany, W. Lu, J.M. Tour, ACS nano, 4 (2010) 4806-4814.

[47] W. Gao, The chemistry of graphene oxide, Graphene oxide, Springer2015, pp. 61-95.

[48] L. Kou, T. Huang, B. Zheng, Y. Han, X. Zhao, K. Gopalsamy, H. Sun, C. Gao, Nat. Commun., 5 (2014) 3754.

[49] G. Xin, T. Yao, H. Sun, S.M. Scott, D. Shao, G. Wang, J. Lian, Science, 349 (2015) 1083-1087.

[50] S. Zhai, C. Wang, H.E. Karahan, Y. Wang, X. Chen, X. Sui, Q. Huang, X. Liao, X. Wang, Y. Chen, Small, 14 (2018) 1800582.

[51] S. Zhai, L. Wei, H.E. Karahan, Y. Wang, C. Wang, A. Montoya, Q. Shao, X. Wang, Y. Chen, Carbon, 132 (2018) 698-708.

[52] G. Qu, J. Cheng, X. Li, D. Yuan, P. Chen, X. Chen, B. Wang, H. Peng, adv. mater., 28 (2016) 3646-3652.

[53] J. Carretero–González, E. Castillo–Martínez, M. Dias–Lima, M. Acik, D.M. Rogers, J. Sovich, C.S. Haines, X. Lepró, M. Kozlov, A. Zhakidov, Adv. Mater., 24 (2012) 5695-5701.

[54] F. Meng, W. Lu, Q. Li, J.H. Byun, Y. Oh, T.W. Chou, Adv. Mater., 27 (2015) 5113-5131.

[55] D. Yu, K. Goh, H. Wang, L. Wei, W. Jiang, Q. Zhang, L. Dai, Y. Chen, Nat. Nanotechnol., 9 (2014) 555.

[56] G. Chen, T. Chen, K. Hou, W. Ma, M. Tebyetekerwa, Y. Cheng, W. Weng, M. Zhu, Carbon, 127 (2018) 218-227.

[57] K. Gopalsamy, Z. Xu, B. Zheng, T. Huang, L. Kou, X. Zhao, C. Gao, Nanoscale, 6 (2014) 8595-8600.

[58] W. Ma, S. Chen, S. Yang, W. Chen, Y. Cheng, Y. Guo, S. Peng, S. Ramakrishna, M. Zhu, J. Power Sources, 306 (2016) 481-488.

[59] W. Ma, S. Chen, S. Yang, W. Chen, W. Weng, Y. Cheng, M. Zhu, Carbon, 113 (2017) 151-158.

[60] Y. Xu, C.-Y. Chen, Z. Zhao, Z. Lin, C. Lee, X. Xu, C. Wang, Y. Huang, M.I. Shakir, X. Duan, Nano Lett., 15 (2015) 4605-4610.

[61] Y. Xu, Z. Lin, X. Zhong, X. Huang, N.O. Weiss, Y. Huang, X. Duan, Nat. Commun., 5 (2014) 4554.

[62] J. Zhang, X. Yang, Y. He, Y. Bai, L. Kang, H. Xu, F. Shi, Z. Lei, Z.-H. Liu, J. Mater. Chem. A, 4 (2016) 9088-9096.

[63] S.H. Aboutalebi, R. Jalili, D. Esrafilzadeh, M. Salari, Z. Gholamvand, S. Aminorroaya Yamini, K. Konstantinov, R.L. Shepherd, J. Chen, S.E. Moulton, ACS nano, 8 (2014) 2456-2466.

[64] S. Pei, H.-M. Cheng, Carbon, 50 (2012) 3210-3228.

[65] S. Yang, A.G. Ricciardulli, S. Liu, R. Dong, M.R. Lohe, A. Becker, M.A. Squillaci, P. Samorì, K. Müllen, X. Feng, Angew. Chem. Int. Ed., 56 (2017) 6669-6675.

[66] S. Pei, Q. Wei, K. Huang, H.-M. Cheng, W. Ren, Nat. Commun., 9 (2018) 145.

[67] X. Wang, G. Sun, P. Routh, D.-H. Kim, W. Huang, P. Chen, Chem. Soc. Rev., 43 (2014) 7067-7098.

[68] J.P. Paraknowitsch, A. Thomas, Energy Environ. Sci., 6 (2013) 2839-2855.

[69] Y. Ma, P. Li, J.W. Sedloff, X. Zhang, H. Zhang, J. Liu, ACS nano, 9 (2015) 1352-1359.

[70] H. Kim, R. Jalili, G.M. Spinks, G.G. Wallace, S.J. Kim, Compos. Sci. Technol., 149 (2017) 280-285.

[71] Z. Liu, Z. Xu, X. Hu, C. Gao, Macromolecules, 46 (2013) 6931-6941.

[72] W. Jiang, S. Zhai, Q. Qian, Y. Yuan, H.E. Karahan, L. Wei, K. Goh, A.K. Ng, J. Wei, Y. Chen, Energy Environ. Sci., 9 (2016) 611-622.

[73] X. Li, X. Li, J. Cheng, D. Yuan, W. Ni, Q. Guan, L. Gao, B. Wang, Nano Energy, 21 (2016) 228-237.

[74] Y. Hu, H. Cheng, F. Zhao, N. Chen, L. Jiang, Z. Feng, L. Qu, Nanoscale, 6 (2014) 6448-6451.

[75] Y. Meng, Y. Zhao, C. Hu, H. Cheng, Y. Hu, Z. Zhang, G. Shi, L. Qu, Adv. Mater., 25 (2013) 2326-2331.

[76] Y. Luo, Y. Zhang, Y. Zhao, X. Fang, J. Ren, W. Weng, Y. Jiang, H. Sun, B. Wang, X. Cheng, J. Mater. Chem. A, 3 (2015) 17553-17557.

[77] P. Li, Z. Jin, L. Peng, F. Zhao, D. Xiao, Y. Jin, G. Yu, Adv. Mater., 30 (2018) 1800124.

[78] W. Yang, L. He, X. Tian, M. Yan, H. Yuan, X. Liao, J. Meng, Z. Hao, L. Mai, small, 13 (2017) 1700639.

[79] X. Hu, W. Zhang, X. Liu, Y. Mei, Y. Huang, Chem. Soc. Rev., 44 (2015) 2376-2404.

[80] G. Sun, X. Zhang, R. Lin, J. Yang, H. Zhang, P. Chen, Angew. Chem. Int. Ed., 54 (2015) 4651-4656.

[81] B. Wang, Q. Wu, H. Sun, J. Zhang, J. Ren, Y. Luo, M. Wang, H. Peng, J. Mater. Chem. A, 5 (2017) 925-930.

[82] X. Wang, G. Sun, P. Routh, D.-H. Kim, W. Huang, P. Chen, Chem. Soc. Rev, 43 (2014) 7067-7098.

[83] M. Acerce, D. Voiry, M. Chhowalla, Nat. Nanotechnol., 10 (2015) 313.

[84] K. Krishnamoorthy, P. Pazhamalai, G.K. Veerasubramani, S.J. Kim, J. Power Sources, 321 (2016) 112-119.

[85] Q. Tang, D.-e. Jiang, Chem. Mater., 27 (2015) 3743-3748.

[86] P. Simon, Y. Gogotsi, B. Dunn, Science, 343 (2014) 1210-1211.

[87] I.-H. Kim, K.-B. Kim, J. Electrochem. Soc., 153 (2006) A383-A389.

[88] Q. Lv, S. Wang, H. Sun, J. Luo, J. Xiao, J. Xiao, F. Xiao, S. Wang, Nano Lett., 16 (2015) 40-47.

[89] X. Xiao, T. Li, P. Yang, Y. Gao, H. Jin, W. Ni, W. Zhan, X. Zhang, Y. Cao, J. Zhong, Acs Nano, 6 (2012) 9200-9206.

[90] L. Lim, Y. Liu, W. Liu, R. Tjandra, L. Rasenthiram, Z. Chen, A. Yu, ACS Appl. Mater. Interfaces, 9 (2017) 39576-39583.

[91] J. Zhang, X. Zhao, Z. Huang, T. Xu, Q. Zhang, Carbon, 107 (2016) 844-851.

[92] N. Yu, H. Yin, W. Zhang, Y. Liu, Z. Tang, M.Q. Zhu, Adv. Energy Mater., 6 (2016) 1501458.

[93] Z. Zhang, F. Xiao, S. Wang, J. Mater. Chem. A, 3 (2015) 11215-11223.

[94] Z. Zhang, F. Xiao, J. Xiao, S. Wang, J. Mater. Chem. A, 3 (2015) 11817-11823.

[95] H. Xu, X. Hu, Y. Sun, H. Yang, X. Liu, Y. Huang, Nano Res., 8 (2015) 1148-1158.

[96] P. Shi, L. Li, L. Hua, Q. Qian, P. Wang, J. Zhou, G. Sun, W. Huang, ACS nano, 11 (2016) 444-452.

[97] X. Cheng, J. Zhang, J. Ren, N. Liu, P. Chen, Y. Zhang, J. Deng, Y. Wang, H. Peng, J. Phys. Chem. C, 120 (2016) 9685-9691.

[98] J. Tao, N. Liu, W. Ma, L. Ding, L. Li, J. Su, Y. Gao, Sci. Rep., 3 (2013) 2286.

[99] Y. Huang, H. Hu, Y. Huang, M. Zhu, W. Meng, C. Liu, Z. Pei, C. Hao, Z. Wang, C. Zhi, ACS nano, 9 (2015) 4766-4775.

[100] M.-J. Deng, F.-L. Huang, I.-W. Sun, W.-T. Tsai, J.-K. Chang, Nanotechnol., 20 (2009) 175602.

[101] W. Luo, X. Hu, Y. Sun, Y. Huang, J. Mater. Chem., 22 (2012) 8916-8921.

[102] H.S. Jadhav, R.S. Kalubarme, C.-N. Park, J. Kim, C.-J. Park, Nanoscale, 6 (2014) 10071-10076.

[103] A. Ramadoss, K.-N. Kang, H.-J. Ahn, S.-I. Kim, S.-T. Ryu, J.-H. Jang, J. Mater. Chem. A, 4 (2016) 4718-4727.

[104] K. Lu, J. Zhang, Y. Wang, J. Ma, B. Song, H. Ma, ACS Sustainable Chem. Eng., 5 (2016) 821-827.

[105] H. Yang, H. Xu, M. Li, L. Zhang, Y. Huang, X. Hu, ACS Appl. Mater. Interfaces, 8 (2016) 1774-1779.

[106] L. Gao, J.U. Surjadi, K. Cao, H. Zhang, P. Li, S. Xu, C. Jiang, J. Song, D. Sun, Y. Lu, ACS Appl. Mater. Interfaces, 9 (2017) 5409-5418.

[107] C. Wu, F. Feng, Y. Xie, Chem. Soc. Rev., 42 (2013) 5157-5183.

[108] L. Hua, Z. Ma, P. Shi, L. Li, K. Rui, J. Zhou, X. Huang, X. Liu, J. Zhu, G. Sun, J. Mater. Chem. A, 5 (2017) 2483-2487.

[109] X. Gong, S. Li, P.S. Lee, Nanoscale, 9 (2017) 10794-10801.

[110] J. Sun, Y. Huang, C. Fu, Y. Huang, M. Zhu, X. Tao, C. Zhi, H. Hu, J. Mater. Chem. A, 4 (2016) 14877-14883.

[111] C. Zhang, B. Anasori, A. Seral-Ascaso, S.H. Park, N. McEvoy, A. Shmeliov, G.S. Duesberg, J.N. Coleman, Y. Gogotsi, V. Nicolosi, Adv. Mater., 29 (2017) 1702678.

[112] M.R. Lukatskaya, S. Kota, Z. Lin, M.-Q. Zhao, N. Shpigel, M.D. Levi, J. Halim, P.-L. Taberna, M.W. Barsoum, P. Simon, Nat. Energy, 2 (2017) 17105.

[113] K. Krishnamoorthy, P. Pazhamalai, S. Sahoo, S.-J. Kim, J. Mater. Chem. A, 5 (2017) 5726-5736.

[114] M. Hu, Z. Li, G. Li, T. Hu, C. Zhang, X. Wang, Adv. Mater. Technol., 2 (2017) 1700143.

[115] J. Zhang, S. Seyedin, Z. Gu, W. Yang, X. Wang, J.M. Razal, Nanoscale, 9 (2017) 18604-18608.

[116] S. Seyedin, E.R.S. Yanza, J.M. Razal, J. Mater. Chem. A, 5 (2017) 24076-24082.

[117] Z. Wang, S. Qin, S. Seyedin, J. Zhang, J. Wang, A. Levitt, N. Li, C. Haines, R. Ovalle-Robles, W. Lei, Small, (2018) 1802225.

[118] L. Ji, Z. Lin, M. Alcoutlabi, X. Zhang, Energy Environ. Sci., 4 (2011) 2682-2699.

[119] Y. Tang, Y. Zhang, W. Li, B. Ma, X. Chen, Chem. Soc. Rev., 44 (2015) 5926-5940.

[120] H.B. Wu, J.S. Chen, H.H. Hng, X.W.D. Lou, Nanoscale, 4 (2012) 2526-2542.

[121] K.-S. Chen, I. Balla, N.S. Luu, M.C. Hersam, ACS Energy Lett., 2 (2017) 2026-2034.

[122] S. Goriparti, E. Miele, F. De Angelis, E. Di Fabrizio, R.P. Zaccaria, C. Capiglia, J. Power Sources, 257 (2014) 421-443.

[123] E. Yoo, J. Kim, E. Hosono, H.-s. Zhou, T. Kudo, I. Honma, Nano Lett., 8 (2008) 2277-2282.

[124] Z.-S. Wu, W. Ren, L. Xu, F. Li, H.-M. Cheng, ACS nano, 5 (2011) 5463-5471.

[125] A. Gerouki, M. Goldner, R. Goldner, T. Haas, T. Liu, S. Slaven, J. Electrochem. Soc., 143 (1996) L262-L263.

[126] P. Lian, X. Zhu, S. Liang, Z. Li, W. Yang, H. Wang, Electrochim. Acta, 55 (2010) 3909-3914.

[127] R. Raccichini, A. Varzi, S. Passerini, B. Scrosati, Nature materials, 14 (2015) 271.

[128] T. Hoshide, Y. Zheng, J. Hou, Z. Wang, Q. Li, Z. Zhao, R. Ma, T. Sasaki, F. Geng, Nano Lett., 17 (2017) 3543-3549.

[129] H. Li, W. Li, L. Ma, W. Chen, J. Wang, J. Alloys Compd., 471 (2009) 442-447.

[130] Y. Luo, Y. Zhang, Y. Zhao, X. Fang, J. Ren, W. Weng, Y. Jiang, H. Sun, B. Wang, X. Cheng, Journal of Materials Chemistry A, 3 (2015) 17553-17557.

[131] M.D. Slater, D. Kim, E. Lee, C.S. Johnson, Adv. Funct. Mater., 23 (2013) 947-958.

[132] S.W. Kim, D.H. Seo, X. Ma, G. Ceder, K. Kang, Adv. Energy Mater., 2 (2012) 710-721.

[133] Y. Wang, D. Kong, S. Huang, Y. Shi, M. Ding, Y. Von Lim, T. Xu, F. Chen, X. Li, H.Y. Yang, J. Mater. Chem. A, 6 (2018) 10813-10824.

[134] Y. Zeng, Y. Meng, Z. Lai, X. Zhang, M. Yu, P. Fang, M. Wu, Y. Tong, X. Lu, Adv. Mater., 29 (2017) 1702698.

[135] Z. Jin, P. Li, Y. Jin, D. Xiao, Energy Storage Mater., 13 (2018) 160-167.

[136] R. Wang, J. Lang, P. Zhang, Z. Lin, X. Yan, Adv. Funct. Mater., 25 (2015) 2270-2278.

[137] P. Sun, R. Lin, Z. Wang, M. Qiu, Z. Chai, B. Zhang, H. Meng, S. Tan, C. Zhao, W. Mai, Nano Energy, 31 (2017) 432-440.

[138] F. Meng, Q. Li, L. Zheng, Energy Storage Mater., 8 (2017) 85-109.

[139] Y. Gogotsi, P. Simon, Science, 334 (2011) 917-918.

[140] B. Wang, X. Fang, H. Sun, S. He, J. Ren, Y. Zhang, H. Peng, Adv. Mater., 27 (2015) 7854-7860.